

Insights into uncertainties in future drought analysis using hydrological simulation model

Jin Hyuck Kim¹, Eun-Sung Chung^{2*}

¹ Department of Civil Engineering, Chungnam National University, 99 Daehak-ro, Yuseong-gu, Daejeon 34134, South Korea.

² Faculty of Civil Engineering, Seoul National University of Science and Technology, 232 Gongneung-ro, Nowon-gu, Seoul 01811, South Korea.

*Corresponding author: Eun-Sung Chung (eschung@seoultech.ac.kr)

Abstract

14 Hydrological analysis utilizing a hydrological model requires a parameter calibration process,
15 which is largely influenced by the length of calibration data period and prevailing hydrological
16 conditions. This study aimed to quantify these uncertainties in future runoff projection and
17 hydrological drought based on future climate data and the calibration data of the hydrological
18 model. Future climate data were sourced from three Shared Socioeconomic Pathway (SSP)
19 scenarios (SSP2-4.5, SSP3-7.0, and SSP5-8.5) of 20 general circulation models (GCMs). The
20 Soil and Water Assessment Tool (SWAT) was employed as the hydrological model, and
21 hydrological conditions were determined using the Streamflow Drought Index (SDI), with
22 calibration data lengths ranging from 1 to 20 years considered. Subsequently, the uncertainty
23 was quantified using Analysis of Variance (ANOVA). After calibrating SWAT parameters, the
24 validation performance was found to be influenced by the hydrological conditions of the
25 calibration data. Hydrological model parameters calibrated using a dry period simulated runoff
26 with 11.4% higher performance in dry conditions and 6.1% higher performance in normal
27 conditions, while hydrological model parameters calibrated using a wet period simulated runoff
28 with 5.1% higher performance in wet conditions. While the ANOVA results confirmed that
29 GCMs are the dominant source of total uncertainty, the uncertainty contribution from the
30 hydrological model calibration in estimating future runoff was analyzed to be 3.9~9.8%,
31 particularly significant in the low runoff period. The uncertainty contribution in future
32 hydrological drought analysis resulting from the calibration of hydrological model parameters
33 was analyzed to be 2.7% on average, which is lower than that of future runoff projection.

35 Key words: Future runoff, Hydrological drought, GCM, SWAT, Uncertainty

36 **1. Introduction**

37 In the current global climate scenarios, characterized by significant warming trends, there are
38 increased challenges in understanding and managing water systems (IPCC, 2014; IPCC, 2021).
39 Water availability for runoff is directly influenced by precipitation, while temperature affects
40 water availability through its effect on evapotranspiration rates (Mahabadi and Delavar, 2024).
41 These climatic changes significantly affect the availability of water resources and increase the
42 occurrence and severity of hydrological extreme events such as floods and droughts in different
43 regions (Milly et al., 2008; Santos et al., 2021). Hydrological projection is crucial for
44 sustainable water resource planning and management (Peng et al., 2022; Yang et al., 2023;
45 Yang et al., 2024). Consequently, quantifying the uncertainty in hydrological projection is
46 essential as it directly affects the effectiveness of these management strategies and decision-
47 making processes in ensuring the reliability and safety of water resources (Zhang et al., 2024).

48 Droughts, which could become more severe due to climate change, begin with a lack of
49 precipitation and lead to a decrease in streamflow and soil moisture deficiency, encompassing
50 a complex hydrological cycle that adversely affects plant and crop growth and human life.
51 Generally, droughts progress over time into meteorological, agricultural, hydrological, and
52 socio-economic droughts, and become a fatal disaster if prolonged (Sheffield and Wood, 2012).
53 Consequently, future droughts due to climate change has been actively conducted, with most
54 studies concluding that droughts are becoming more frequent and severe (Sung et al., 2018;
55 Kim et al., 2021).

56 Hydrological drought requires an understanding of the hydrological cycle, including runoff,
57 surface water, and groundwater. Runoff, a key indicator of hydrological drought, significantly
58 affects the availability of water for agricultural, industrial, and domestic uses (Ghasemizade
59 and Schirmer, 2013; Devia et al., 2015). Therefore, understanding and predicting runoff
60 behavior is essential for hydrological drought analysis in water resource management and
61 planning. While runoff data can be obtained from river observations within the region, there
62 are limitations in observation technology and coverage. Consequently, simulated runoff data
63 using regional meteorological data and hydrological models are utilized. Hydrological models
64 simulate runoff by inputting meteorological data, soil data, and topographical data, allowing
65 for the prediction of future hydrological cycles. However, these hydrological models are
66 influenced by various factors, including the quality and quantity of input data, structural
67 uncertainties of the models, and uncertainties in the calibration process (Xu et al., 2007; Renard

68 et al., 2010). Therefore, quantifying and recognizing these uncertainties is crucial to enhancing
69 the reliability of future hydrological analysis (Feng et al., 2019).

70 The future hydrological analysis considering uncertainty is essential for effective water
71 management. These projections are largely based on General Circulation Models (GCMs) and
72 hydrological models, which are critical tools for modelling the hydrological impacts of climate
73 change. However, GCMs introduce significant uncertainty in future runoff prediction due to
74 their inherent structural complexity and variability in scenario-based inputs (Broderick et al.,
75 2016). This uncertainty has a direct impact on the accuracy of runoff predictions and poses a
76 significant challenge to water resource management. The selection and use of GCMs have a
77 crucial role in shaping these uncertainties, making the consideration of a variety of GCMs and
78 shared socioeconomic pathways (SSP) scenarios essential for managing uncertainties and
79 improving projections (Vetter et al., 2015; Chae et al., 2024a). Indeed, Shi et al. (2022) had
80 shown how different evapotranspiration models embedded in GCMs affect runoff prediction,
81 highlighting GCMs and Representative Concentration Pathways (RCPs) as major factors
82 affecting uncertainty. Similarly, Lee et al. (2021a) had shown how the choice of GCMs
83 significantly affects prediction of water storage in wetlands under future climate scenarios. To
84 understand these uncertainties, Wang et al. (2020) suggested the use of a broad ensemble of at
85 least 10 GCMs, which allowed for a more comprehensive assessment of hydrological impacts
86 and helped to reduce the inherent uncertainties associated with climate change. Thus, the use
87 of a wide range of GCMs is an essential strategy for maximizing the effectiveness of water
88 resource management under global climate change conditions.

89 The hydrological model calibration involves significant uncertainty, especially when
90 predicting future conditions. This process, crucial for aligning model parameters with historical
91 data, often incorrectly assumes that parameters validated under past hydrological conditions
92 will remain valid in the future. Thirel et al. (2015) and Fowler et al. (2016) demonstrated that
93 models calibrated with historical climate data might not perform accurately under changed
94 conditions, leading to substantial uncertainties in runoff projections. This challenge is
95 exacerbated by the dependency of model parameters on the hydrological conditions prevalent
96 during the calibration period (Merz et al., 2011; Coron et al., 2012). Effective calibration
97 strategies, therefore, must consider variable climate scenarios to ensure model robustness. This
98 involves rigorous calibration under diverse conditions to validate hydrological models'
99 reliability in projecting future water resource availability (Saft et al., 2016; Dakhlaoui et al.,
100 2017). Furthermore, the interaction between model parameters and hydrological conditions

101 during these periods often complicates the calibration process, underscoring the need for robust
102 validation techniques. The duration of the calibration period also contributes significantly to
103 the uncertainty in runoff projection. Razavi and Tolson (2013) and Arsenault et al. (2018)
104 highlighted the importance of sufficiently long calibration periods to ensure meaningful
105 calibration and validation results. In addition, Kim et al. (2011) cautioned against using overly
106 short calibration periods, as this can lead to large and unstable model performance variability
107 during calibration and validation. Despite the emphasis on longer calibration periods, Perrin et
108 al. (2007), Sun et al. (2017), Yu et al. (2023), and Ziarh et al. (2024) had found that an extended
109 calibration data length does not guarantee improved model performance, suggesting a nuanced
110 approach to calibration period selection. These insights underlined the complex interplay
111 among calibration length, model parameter selection, and climatic variability in shaping the
112 reliability of hydrological models.

113 The rigorous quantification of uncertainties in hydrological modeling is essential to enhance
114 the reliability of water resources planning and management. This study employs Analysis of
115 Variance (ANOVA), a statistical method widely used in hydrological studies, to systematically
116 quantify uncertainties in hydrological projections. ANOVA dissects the variance observed in
117 projections into contributions from various sources of uncertainty, such as GCM outputs, SSP
118 scenarios, and hydrological model parameters (Qi et al., 2016; Chae et al., 2024b). By
119 identifying the dominant sources of variability and analyzing their interactions, ANOVA
120 provides a clear understanding of how different factors drive uncertainties in hydrological
121 projections. Recent applications of ANOVA in future hydrological studies demonstrated its
122 effectiveness in understanding model-driven uncertainties (Chen et al., 2022; Yuan et al., 2022;
123 Mo et al., 2024).

124 This study focuses on the uncertainty in future hydrological analyses, which are influenced by
125 hydrological model parameters during different calibration periods under future climate data
126 and different hydrological conditions. This research utilizes the Soil and Water Assessment
127 Tool (SWAT), a widely recognized hydrological model, to analyze the impact of hydrological
128 conditions during the calibration period on the projection of future runoff and hydrological
129 drought. Three SSP scenarios and 20 GCMs were used to consider uncertainty due to future
130 climate, and different hydrological conditions according to the Streamflow Drought Index (SDI)
131 and different calibration period data lengths from 1 to 20 years were used to consider
132 uncertainty in hydrological model parameter calibration. This study aims to contribute to the

133 refinement of hydrological modelling practices by quantifying the uncertainties associated with
134 future runoff projection and hydrological drought analysis.

135 This manuscript is structured as follows. In Section 2, the study area, datasets, and the
136 methodologies used in this study are described, including SWAT, the ANOVA framework, and
137 the statistical validation procedures. In Section 3, the results of the analysis are presented,
138 showing the effects of calibration conditions on model performance and quantifying the
139 uncertainty contributions from various sources for both future runoff and hydrological drought.
140 In Section 4, the implications of these findings are discussed in the context of previous research.
141 Finally, Section 5 summarizes the main conclusions of this study.

142

143 **2. Methodology**

144 **2.1 Procedure**

145 The procedure of the study is as follows. The overall workflow, illustrating the main phases of
146 data processing, model setup, and analysis, is visualized in Fig. 1. First, topographic data for
147 four dam basins in South Korea were established, taking into account the overall hydrological
148 characteristics of the region, and observed dam inflow data were utilized to consider the length
149 and hydrological conditions of the hydrological model calibration data. The length of the
150 calibration data considered ranged from 1 to 20 years, and hydrological conditions were
151 categorized using the Streamflow Drought Index (SDI). Subsequently, validation performance
152 analysis was conducted, with calculations varying according to the length of calibration data
153 and hydrological conditions (Dry, Normal, and Wet). For the study, future climate data from
154 20 Coupled Model Intercomparison Project Phase 6 (CMIP6) GCMs and three SSP scenarios
155 (SSP2-4.5, SSP3-7.0, and SSP5-8.5) were bias-corrected. Future runoff projection and
156 hydrological drought were then analyzed using calibrated hydrological model parameters under
157 different conditions along with the future climate data. Finally, the uncertainties in the future
158 hydrological analysis were quantified using the Analysis of Variance (ANOVA).

159

160 **2.2 Study area and datasets**

161 The study areas selected in this study are the Andong (AD), Chungju (CJ), Habcheon (HCH),
162 and Seomjingang (SJ) dam basins located in Korea as shown in Fig. 2. To achieve stable

163 calibration and validation results for a hydrological model, it is imperative to choose
164 catchments with extensive hydrological data records. This enables the accurate estimation of
165 appropriate calibration data lengths through various testing periods of the hydrological model.
166 Furthermore, incorporating a variety of basins is crucial to ensure that the findings of this study
167 are not biased by specific hydrological conditions. These four basins, which have the longest
168 hydrological records in Korea, are situated in major river basins. Detailed basin characteristics
169 are provided in Table S1. While all four basins are located in temperate climate zones and are
170 predominantly forested (Forest ratio > 75%, except for CJ at 61.7%), they represent a diverse
171 range of hydrological and climatic conditions. While all four basins are located in temperate
172 climate zones and are predominantly forested (Forest ratio > 75%, except for CJ at 61.7%),
173 they represent a diverse range of hydrological and climatic conditions. Area varies significantly
174 from 763 km² (SJ) to 6,648 km² (CJ). Mean annual precipitation also ranges from 1,045.7 mm
175 (AD) to 1,329.8 mm (SJ). These regions are devoid of artificial structures (Urban ratio < 5.3%
176 for all basins), ensuring that runoff remains natural and unaltered. Located in different regions
177 of Korea, these basins have a range of hydrological conditions and runoff characteristics,
178 providing a representative cross-section of the country's hydrological characteristics.

179

180 **2.3 Soil and water assessment tool (SWAT)**

181 SWAT was used to calibrate hydrological processes in our study basin. SWAT is particularly
182 adept at simulating runoff and other hydrological variables under a wide range of
183 environmental conditions and is a robust, physically based, semi-distributed model. Its
184 efficiency in modelling hydrological cycles within basins relies on simple input variables to
185 produce detailed hydrological outputs. The capability of this model has been effectively shown
186 in various studies, including those in South Korea (Kim et al., 2022; Song et al., 2022).

187 The core of SWAT is the water balance equation, which integrates daily weather data with land
188 surface parameters to calculate water storage changes over time:

189

$$190 SW_t = SW_0 + \sum_{i=0}^t (R_{day} - Q_{surf} - E_a - w_{seep} - Q_{gw}) \quad (1)$$

191

192 where SW_0 is the initial soil moisture content (mm), SW_t is the total soil moisture per day
193 (mm), R_{day} is precipitation (mm), Q_{surf} is surface runoff (mm), E_a is evapotranspiration
194 (mm), W_{seed} is penetration, Q_{gw} is groundwater runoff (mm), and t is time (day).

195 For rainfall-runoff analysis, SWAT is structured into several sub-basins, each of which is
196 further subdivided into Hydrologic Response Units (HRUs) based on different soil types, land
197 use and topography. Each HRU independently simulates parts of the hydrological cycle,
198 allowing a granular analysis of basin hydrology. This setup reflects the spatial heterogeneity
199 within the basin and allows continuous simulation of hydrological processes over long time
200 periods, enhancing the utility of the model for climate change studies. The model was
201 calibrated and validated using R-SWAT for parameter optimization. R-SWAT incorporates the
202 SUFI-2 algorithm, which is known for its rapid execution and precision in parameter
203 optimization, ensuring accurate and reliable simulation results (Nguyen et al., 2022). In this
204 study, the setup and evaluation of SWAT for the historical period were performed using
205 observed data. The model was forced with observed meteorological data, and the parameters
206 were calibrated and validated against historical daily dam inflow records for the period 1980-
207 2023.

208

209 **2.4 Streamflow drought index (SDI)**

210 The drought index was used to classify hydrological conditions considering the calibration
211 effect of periods with different hydrological conditions. SDI is a commonly used method for
212 quantifying the severity and duration of drought conditions in a river basin. It is based on the
213 comparison of observed streamflow with a historical reference period, usually the average
214 streamflow over a long-term period. SDI which is a hydrological drought index, is calculated
215 as Eq. 2. (Nalbantis and Tsakiris, 2009).

216

$$217 SDI_{i,k} = \frac{V_{i,k} - \bar{V}_k}{S_k} \quad (2)$$

218

219 where $V_{i,k}$ is the runoff accumulated during the k th period in the i th year, and \bar{V}_k and S_k
220 represent the average and standard deviation of the accumulated river flow, respectively.

221 The critical level is mainly the average \bar{V}_k . In small scale rivers, the runoff rate approximates
222 the Log-normal distribution type and the probability distribution type is distorted. Therefore,
223 the runoff rate must be converted to fit the normal distribution. When converting to a two-
224 variable log-normal distribution type, SDI is finally equal to Eq. 3, and $y_{i,k}$ is a value obtained
225 by taking the natural logarithm of the amount of river water, such as Eq. 4.

226

227
$$SDI_{i,k} = \frac{y_{i,k} - \bar{y}_k}{S_{y,k}}, i = 1,2, \dots, k = 1,2,3,4 \quad (3)$$

228

229
$$y_{i,k} = \ln(V_{i,k}), I = 1,2, \dots, K = 1,2,3,4 \quad (4)$$

230

231 To classify the hydrological conditions, this study categorized -0.5 and below as Dry, 0.5 and
232 above as Wet, and -0.5 to 0.5 as Normal (Nalbantis and Tsakiris, 2009; Hong et al., 2015).

233

234 **2.5 General Circulation Models (GCMs)**

235 In this study, M1 to M20 GCMs from the CMIP6 suite that have been consistently used in
236 studies for East Asia and Korea were selected for future runoff projection and hydrological
237 drought analysis. The details of the development institutions, model names and resolutions of
238 these 20 GCMs were presented in Table S2.

239 The climate data from the GCMs were evaluated using daily observed climate data provided
240 by the Korea Meteorological Administration (KMA). The evaluation used observed data from
241 the past period (1985-2014) to evaluate the future climate data from the GCMs, which were
242 analyzed for two future periods: the near future (NF) and the distance future (DF). The future
243 climate change scenarios used were SSP2-4.5, SSP3-7.0 and SSP5-8.5. The SSP scenarios are
244 divided into five pathways based on radiative forcing, reflecting different levels of future
245 mitigation and adaptation efforts (O'Neill et al., 2016). The SSPs are numbered from SSP1 to
246 SSP5, with SSP1 representing a sustainable green pathway and SSP5 representing fossil fuel
247 driven development. The numbers 4.5 to 8.5 indicate the level of radiative forcing (4.5: 4.5 W
248 m⁻², 7.0: 7.0 W m⁻² and 8.5: 8.5 W m⁻²). For the analysis of future changes, the calibrated
249 SWAT was then driven by bias-corrected future climate projection data from the 20 GCMs

250 under the three SSP scenarios. This approach ensures that the model's baseline performance is
251 grounded in observational data, while the future analysis specifically assesses the uncertainties
252 propagated from the climate projections and hydrological modeling choices.

253

254 **2.6 Bias correction using quantile mapping**

255 The GCMs data outputs in a gridded format with a fixed resolution, requiring the use of spatial
256 interpolation methods. In this study, the inverse distance weighting (IDW) method was
257 employed to spatially interpolate the GCM data based on the locations of the Korea
258 Meteorological stations. Subsequently, to align the GCM data with the actual observational
259 data, the quantile mapping method was utilized. This method adjusts the GCM data based on
260 the quantile relationship between the cumulative distribution functions (cdf) of the GCM data
261 and the observed data (Gudmundsson et al., 2012). The quantile mapping method is described
262 by Eq (5).

263

264
$$P_o = F_o^{-1}(F_m(P_m)) \quad (5)$$

265

266 where, P_o and P_m represent observed and simulated climate variables, F_m is the CDF of P_m
267 and F_o^{-1} is the inverse CDF corresponding to P_o .

268 The quantile relationship can be also derived directly using parametric transformations. In this
269 study, the linear method of parametric transformation was adopted as Eq. (6).

270

271
$$\hat{P} = a + bP_m \quad (6)$$

272

273 where, \hat{P} represents the best estimate of P_o and a and b are free parameters that are subject
274 to calibration.

275

276 **2.7 Quantifying uncertainty**

277 The ANOVA used in this study is an effective statistical method that decomposes the total sum
278 of squares (SST) into contributions from different sources and their interactions. This method
279 would be particularly useful in the study framework, as it allows us to assess not only the
280 individual effects of each source of uncertainty but also the combined effects of these sources
281 interacting with each other (Bosshard et al., 2013; Lee et al., 2021a).

282 For this analysis, the primary sources of uncertainty considered are General Circulation Models
283 (GCMs), Shared Socioeconomic Pathway (SSP) scenarios, hydrological conditions (HC)
284 during the calibration period, and period length (PL). Each of these sources could have a
285 significant impact on the projections of hydrological models; therefore, their comprehensive
286 evaluation is crucial (Morim et al., 2019; Yip et al., 2011). Higher-order interactions (e.g.,
287 three-way) were excluded as they are often difficult to interpret physically and can introduce
288 noise into the model.

289

$$290 SST = SS_{GCMs} + SS_{SSPs} + SS_{HC} + SS_{PL} + SS_{Interactions(2-way)} + SS_{Residuals} \quad (7)$$

291

292 where each term (SS) indicates the sum of squares attributed to each factor or interaction.
293 Here, SS_{GCMs} , SS_{SSPs} , SS_{HC} , and SS_{PL} represent the sum of squares due to GCMs, SSPs, HC,
294 and PL, respectively, known as the main effects. The remaining terms represent the sum of
295 squares due to the interactions among GCMs, SSPs, hydrological conditions, period length,
296 their two-way interactions, and the residual error.

297 The model setup for ANOVA was designed to analyze the set of projections. As detailed in the
298 flowchart (Fig. 1), this set was generated by combining 60 climate data (20 GCMs \times 3 SSPs)
299 with 60 distinct hydrological model parameterization (3 HC \times 20 PL). This resulted in a total
300 of 3,600 combinations for each basin analyzed. Initially, the SST, representing the total
301 variation within the data, was calculated. Subsequently, the sum of squares attributable to each
302 source of uncertainty was computed. To quantify the relative impact of each source, its
303 contribution was calculated as the proportion of its Sum of Squares relative to the Total Sum
304 of Squares. This provides a clear measure of the percentage of total uncertainty explained by
305 each factor and interaction.

306 The statistical robustness and validity of the ANOVA models were rigorously evaluated. First,
307 the overall goodness-of-fit for each model was assessed using the Adjusted R-squared (R_{adj}^2),
308 defined as Eq. (8).

309

310
$$R_{adj}^2 = 1 - \frac{(1-R^2)(n-1)}{n-k-1} \quad (8)$$

311

312 Where, R^2 is the coefficient of determination, n is the number of observations, and k is the
313 number of predictions. This metric is preferred over the Standard R-squared as it adjusts for
314 the number of predictors in the model, providing a more accurate measure of model fit.

315 Second, a residual analysis was conducted to verify that the core assumptions of ANOVA were
316 met. The normality of residuals was a primary focus of this validation, examined both
317 statistically with the Shapiro-Wilk test and visually using Quantile-Quantile (Q-Q) plots. The
318 Shapiro-Wilk test evaluates the null hypothesis that the residuals are normally distributed.
319 However, given the large sample size in this study, which can lead to statistically significant
320 results even for minor deviations from normality, greater emphasis was placed on the visual
321 inspection of Q-Q plots to assess practical adherence to the normality assumption. The
322 assumption of homoscedasticity (constant variance of residuals) was also inspected using
323 Residuals vs. Fitted values plots. These validation steps ensure that the results of the
324 uncertainty partitioning are statistically sound and reliable. All statistical analyses were
325 performed using the R software environment.

326

327 **3. Results**

328 **3.1 Determining the hydrological conditions**

329 The calculated SDI was shown in Fig. S. 1. The SDI values of AD and HCH in the Nakdong
330 River basin showed drought conditions similar to the actual events that occurred in 1994-1995,
331 2009, 2014-2015, 2016, 2017 and 2022 (Karunakalage et al., 2024). Similarly, SDI values of
332 CJ in the Han River basin accurately reflected the actual drought events of 2014-2015 and 2017
333 (Lee et al., 2021b). Finally, those of SJ in the Seomjin River basin also represented the drought
334 events of 1995, 2005-2006 and 2018-2019, demonstrating that the SDI was accurately

335 calculated. Therefore, this study using the observed inflow data of the four basins could reflect
336 the hydrological drought characteristics of the historical periods in South Korea.

337

338 **3.2 SWAT parameter calibration**

339 The simulated runoff data were analyzed for performance using the Kling-Gupta Efficiency
340 (KGE; Gupta et al., 2009). KGE was developed to overcome some limitations of the commonly
341 used Nash-Sutcliffe Efficiency (NSE) in performance analysis (Gupta et al., 2009). The
342 attributes of KGE include focusing on a few basic required properties of any model simulation:
343 (i) bias in the mean, (ii) bias in the variability, and (iii) cross-correlation with the observational
344 data (measuring differences in hydrograph shape and timing). The parameter optimization of
345 SWAT was performed using 20 different data lengths, from 1 to 20 years. The specific for
346 these calibration periods, illustrating which historical years correspond to each length, is
347 schematically shown in Fig. S. 2. A rigorous validation scheme was adopted to prevent bias
348 from specific period characteristics and to ensure a robust evaluation of predictive performance.
349 For any given calibration period, the validation was not performed on the entire remaining
350 period as a single dataset. Instead, we conducted a year-by-year validation, calculating a
351 separate KGE value for each individual year not included in the calibration set. For instance, if
352 a model was calibrated on years 1-5 from a 20-year record, 15 distinct single-year KGE values
353 were calculated for years 6 through 20. This approach strictly separates calibration and
354 validation datasets and ensures that model performance is assessed across a diverse range of
355 annual hydrological conditions, providing a robust foundation for the subsequent uncertainty
356 analysis.

357 Following parameter optimization, KGE values as shown in Fig. 3 were found to be suitable
358 for conducting the study, with all four dam basins achieving values above 0.60. The
359 performance improvements are as follows: AD's KGE increased from 0.55 before calibration
360 to 0.64 after calibration, CJ's from 0.68 to 0.75, HCH's from 0.70 to 0.80, and SJ's from 0.50
361 to 0.73. This improvement in KGE after calibration underscores the robustness of the
362 hydrological models used and their enhanced capability in projecting future runoff.

363

364 **3.3 Effect of varying data length**

365 The validation performance according to the calibration data length was shown in Fig. 4. The
366 impact of calibration data length on validation performance was analyzed, revealing a departure

367 from previous studies, which suggested that longer calibration data lengths lead to more
368 effective optimization of hydrological model parameters. Instead, the influence of calibration
369 data length on performance is all different by basin. For AD, the best performance was
370 observed with a 2-year period, averaging a KGE of 0.66, while the 1-year period resulted in
371 the lowest performance with an average KGE of 0.48. The Inter Quartile Range (IQR) showed
372 that variations were smaller for periods longer than 10 years (average IQR of 0.15) compared
373 to those less than 10 years (average IQR of 0.20). For CJ, the optimal performance was at a 15-
374 year period with an average KGE of 0.72, and the lowest at a 4-year period with an average
375 KGE of 0.58. The IQR values were 0.19 for periods under 10 years and 0.20 for periods over
376 10 years, indicating minor differences due to length. For HCH, the highest KGE of 0.77 was
377 recorded at 19 years, and the lowest KGE of 0.66 at 1 year. The IQR for periods under 10 years
378 was 0.19, and 0.10 for those over 10 years, showing that longer periods yielded less variability.
379 In the case of SJ, a 9-year period had a KGE of 0.68, and a 20-year period had a KGE of 0.60,
380 with IQRs of 0.23 for periods under 10 years and 0.21 for those over. While the best validation
381 performance due to calibration data length varied by basin, it was observed that the differences
382 due to the period decrease as the length increases.

383

384 **3.4 Effect of varying hydrological conditions**

385 The performance analyses based on the hydrological conditions of the calibration and
386 validation periods are shown in Fig. S. 3 and Table 1. Fig. S. 3 shows the KGE values and the
387 confidence level (prediction) for each hydrological condition during the validation period
388 according to the SDI values. Overall, during the dry and normal validation periods, it was
389 analyzed that lower SDI values (dry condition) correlated with higher KGE values. This
390 indicates that SWAT parameters calibrated with dry validation period data effectively simulate
391 runoff under Dry and Normal hydrological conditions. For wet validation periods, higher SDI
392 values (wet condition) correlate with higher KGE values, indicating that SWAT parameters
393 calibrated with wet calibration period data accurately simulate runoff under wet conditions.

394 As shown in Table 1, the average KGE according to hydrological conditions is as follows. The
395 KGE values for each dam basin, according to the hydrological conditions of the calibration-
396 validation periods, are as follows: For AD, D-D (Dry-Dry; hydrological conditions for
397 calibration and validation periods, respectively) was 0.480, higher than W-D (Wet-Dry) of
398 0.382; D-N (Dry-Normal) was 0.573, higher than W-N (Wet-Normal) of 0.510; and W-W

399 (Wet-Wet) was 0.642, higher than D-W (Dry-Wet) of 0.571. For CJ, D-D was 0.743, higher
400 than W-D at 0.725; D-N was 0.643, higher than W-N at 0.615; and W-W was 0.706, higher
401 than D-W at 0.674. For HCH, D-D was 0.732, higher than W-D at 0.670; D-N was 0.738,
402 higher than W-N at 0.714; and W-W was 0.769, higher than N-W (Normal-Wet) at 0.757.
403 Lastly, for SJ, D-D was 0.557, higher than W-D at 0.515; D-N was 0.677, higher than W-N at
404 0.650; and W-W was 0.684, higher than D-W at 0.674.

405 The performance evaluation classified by data length and hydrological conditions for validation
406 are influenced by hydrological conditions for calibration, but the optimal data length for the
407 best performance varies between basins as shown in Fig. 5. These results confirm the
408 importance of uncertainty in hydrological models due to differences in hydrological conditions
409 during the calibration and validation periods, as suggested by previous studies (Bai et al., 2022;
410 Fowler et al., 2016). Furthermore, the different data lengths with high validation performance
411 for each basin confirm the opinion that shorter calibration data lengths can be applied under
412 limited data conditions (Perrin et al., 2007; Yu et al., 2023), instead of the traditional opinion
413 that longer calibration data lengths are better for hydrological modelling (Arsenault et al., 2018;
414 Kim et al., 2011).

415

416 **3.5 Bias correction for GCMs**

417 In this study, climate data from GCMs were bias-corrected using observed climate data from
418 KMA weather stations located within each dam basin. Fig. S. 4 describes the root mean square
419 error (RMSE), Pearson coefficient and standard deviation (SD) in a Taylor diagram. After bias
420 correction, all GCMs' climate data showed improved performance. The Pearson coefficient of
421 precipitation increased from 0.04 to 0.99 and the RMSE decreased from 4.43 to 0.05. Similarly,
422 the Pearson coefficients of the daily maximum and minimum temperatures averaged 1.00 and
423 their RMSEs averaged 0.08. This is an indication that the GCM's climate data after bias
424 correction were appropriate for use in this study.

425

426 **3.6 Projection of climate variable**

427 The future climate data from bias-corrected GCMs were depicted in Fig. 6 and Table S3. The
428 future period was divided into NF and FF, and it was found that daily precipitation, maximum
429 temperature, and minimum temperature all increased overall. Except for July and August,
430 future precipitation generally increased, with significant rises particularly noted in April and

431 May. In NF, the largest increase occurred in May under SSP2-4.5 with 51.4 mm, while in DF,
432 the largest increase occurred in April under SSP5-8.5 with 59.8 mm. The largest decrease in
433 NF was calculated for July under SSP5-8.5, and in DF it was most significant under SSP3-7.0,
434 indicating considerable uncertainties in the GCMs during July and August, the months of the
435 highest precipitation.

436 With regard to maximum temperatures, the analysis shows that there has been an increase in
437 all months except April in NF, especially in fall (September-November). This increase was
438 more pronounced in the DF than in the NF, with the largest increases observed under SSP5-
439 8.5. Similarly, the minimum temperature was found to have increased in the future compared
440 to the past, following the same trend as the maximum temperature.

441

442 **3.7 Projection future runoff**

443 3.7.1 Annual runoff change

444 The future runoff was projected using climate data and hydrological model parameters as
445 shown in Fig. S. 5. Overall, future runoff is expected to increase relative to the historical data,
446 with more significant increases projected during DF than NF. As the SSPs change (e.g. from
447 SSP2-4.5 and SSP3-7.0 to SSP5-8.5), not all annual runoff show a consistent increase with the
448 scenario change, as shown in Table 2. In particular, the increase in annual runoff under SSP5-
449 8.5 was not always higher than SSP2-4.5 or SSP3-7.0. These differences were analyzed to vary
450 significantly between different basins and GCMs.

451 For AD, the future seasonal runoff is likely to increase in all seasons except summer. This
452 increase would be more pronounced during DF than NF, with the largest increases occurring
453 under SSP5-8.5. For CJ, the future runoff is expected to increase compared to the past in all
454 seasons, with the highest increase observed in DF under SSP3-7.0 and the lowest increase
455 under SSP5-8.5. For HCH, future runoff is expected to increase in all seasons except fall, with
456 the greatest variability in fall under SSP3-7.0. For SJ, future runoff is projected to increase
457 compared to the past in all scenarios except NF under SSP3-7.0.

458

459 3.7.2 Differences in projected future runoff due to hydrological model parameters

460 The future runoff projections using many calibrated sets of hydrological model parameters
461 were analyzed using the flow duration curve (FDC). In water resources planning and drought
462 management, the differences in future runoff projections due to hydrological model parameters
463 at low runoff are critical. These differences are shown in Fig. S. 6, and the differences in Q75
464 for each basin and their proportions relative to the mean runoff are shown in Table 3. The basin
465 with the largest differences due to hydrological conditions in the calibration period was
466 analysed as HCH. HCH is a basin with relatively low precipitation and a small watershed area.
467 CJ, the largest basin, was analysed to have a 5-6% difference in runoff by hydrological model
468 parameters, which means that the effect of hydrological model calibration is larger in smaller
469 basins. The overall trend shows larger variances in DF than NF, and these variances were more
470 pronounced for SSP5-8.5 scenario than SSP2-4.5. This indicates the need to consider the
471 variations caused by hydrological model parameters when managing water resources during
472 both flood and drought periods. Table S4 details the top three GCMs that showed the most
473 significant differences in runoff projections due to hydrological model parameters for each
474 basin. Models, M5 and M6 were consistently identified as having the largest discrepancies in
475 future runoff projections due to hydrological model parameters.

476

477 **3.8 Uncertainty contribution of future runoff projections**

478 3.8.1 Statistical significance of ANOVA results for future runoff projection

479 Before assessing the significance of individual uncertainty sources, the statistical validity of
480 the developed ANOVA models was confirmed. The goodness-of-fit for all monthly models
481 across all four basins and both future periods (NF and DF) were exceptionally high, with
482 Adjusted R-squared values consistently exceeding 0.99. This indicates that the selected factors
483 and their two-way interactions explain more than 99% of the variance in the projected future
484 runoff. Furthermore, a comprehensive residual analysis was conducted for each model. While
485 statistical tests for normality, such as the Shapiro-Wilk test, are sensitive to large sample sizes,
486 the visual inspection of Q-Q plots and Residuals vs. Fitted plots confirmed that the assumptions
487 of normality and homoscedasticity were practically satisfied, ensuring the reliability of the
488 subsequent significance testing (Fig. S. 7-8).

489 The factors related to the hydrological model calibration, HC and PL, were also found to be
490 statistically significant for the future runoff projections. Table 4-5 summarizes the frequency
491 of statistical significance ($p < 0.05$) for each factor across the four study basins. The values

492 indicate the number of basins out of four where the factor was found to be significant. Although
493 their influence was smaller than that of GCMs and SSPs, both HC and PL were significant (p
494 < 0.05) in numerous months, particularly during the low-flow periods such as spring and winter.
495 This result highlights that the calibration conditions should be considered an important source
496 of uncertainty.

497 Among the two-way interactions, the GCM:SSP interaction consistently showed the highest
498 statistical significance ($p < 0.001$) across all months and basins, indicating that the effect of a
499 GCM is strongly dependent on the chosen SSP scenario, and vice versa. Furthermore,
500 interactions involving the calibration factors, such as GCM:HC and HC:PL, were also found
501 to be statistically significant in various months. This finding is crucial as it demonstrates that
502 the uncertainty stemming from hydrological model calibration does not act in isolation but
503 interacts in a complex manner with future climate projections, thereby influencing the overall
504 uncertainty of future runoff.

505

506 3.8.2 Contribution of uncertainty using the ANOVA

507 A comprehensive overview of the relative contributions from all factors to the uncertainties in
508 future runoff projections for each basin is provided in Fig. S. 9. As confirmed in Fig. S. 9, the
509 differences in future climate data from the GCMs were found to be the largest source of
510 uncertainty, consistently contributing over 60%. This contribution is more significant during
511 NF than DF, as discussed in Section 3.6. Fig. 6 specifically highlights the uncertainty
512 contributions attributed to hydrological models.

513 The uncertainty contributions from hydrological models were most significant during the
514 spring (Mar-May) and winter (Dec-Feb) periods, as shown in Table S5. The results of the
515 analysis for each basin were as follows: For AD, the hydrological model uncertainty was most
516 significant in spring (NF: 7.54%, and DF: 5.86%), with a maximum of 9.76% in June for NF
517 and 7.54% in April for DF. In CJ, the highest uncertainties were also found for NF in winter
518 (3.9%) and for DF in spring (3.96%). HCH showed the highest uncertainty in winter (NF:
519 6.09%, and DF: 5.5%), with a maximum in November (NF: 9.76%, and DF: 8.92%). For SJ,
520 the most significant contributions were found in spring (NF: 5.58%, and DF: 3.88%). In the
521 end, hydrological model uncertainties were more significant in months with lower runoff.

522

523 **3.9 Future hydrological drought uncertainty**

524 3.9.1 Future hydrological drought uncertainty according to hydrological conditions

525 To quantify the uncertainty in the future hydrological drought analysis using the calibrated sets
526 of hydrological model parameters, the Streamflow Drought Index (SDI) was used to calculate
527 the hydrological drought conditions during the future period. For the uncertainty analysis,
528 runoff data were considered for both historical and future periods. Table 6 shows the difference
529 in the number of drought events under hydrological conditions during the calibration period
530 after calculating SDIs for 3-month, 6-month, and 12-month durations. The difference in the
531 number of drought events according to the hydrological conditions of the calibration period
532 was analysed differently for each SSP and basin. The difference was significant for the shorter
533 duration of 3 months.

534 According to the analysis by basin, the difference in the number of drought events in the AD
535 basin with a 3-month duration was calculated to be the largest, with an average of 4.93 events,
536 followed by SJ, CJ, and HCH. Between the near future (NF) and distant future (DF), the
537 difference in the number of drought events under the overall hydrological conditions was larger
538 in the NF, and this difference was calculated differently by basin, confirming the need for
539 basin-specific analysis in water resource management planning. Therefore, the uncertainty
540 quantification of the drought analysis was performed using the SDI with a duration of 3 months.

541

542 3.9.2 Statistical significance of ANOVA results for future hydrological drought

543 To confirm the statistical validity of the ANOVA models for the future hydrological drought
544 analysis, the goodness-of-fit was evaluated. The models showed a high goodness-of-fit, with
545 Adjusted R-squared values consistently greater than 0.99 for all annual models across the four
546 basins. This indicates that the selected factors and their two-way interactions explain more than
547 99% of the variance in the future drought projections, ensuring the reliability of the analysis.

548 Table 7 summarizes the frequency of statistical significance ($p < 0.05$) for each factor,
549 aggregated by decade, to provide a concise overview of the results across the entire future
550 period. The values indicate the number of basins (out of four) where the factor was found to be
551 significant for the majority of years within that decade. The primary climate-related factors,
552 GCM and SSP, were consistently identified as the most significant sources of uncertainty. As
553 shown in Table 7, both factors were found to be highly significant across all four basins for all

554 decades, underscoring the profound impact of climate model choice and emission scenarios on
555 drought projections.

556 The hydrological model calibration factors, HC and PL, also proved to be important sources of
557 uncertainty. Both factors were statistically significant across all four basins for the entire future
558 period. This finding reinforces that the hydrological conditions and data length used for model
559 calibration have a persistent and significant influence on long-term hydrological drought
560 assessments.

561 Regarding the interaction effects, the GCM:SSP interaction was the most consistently
562 significant, highlighting that the projected drought severity under a specific GCM is highly
563 dependent on the emission scenario. Moreover, interactions involving calibration factors,
564 particularly GCM:HC, GCM:PL, and HC:PL, were also found to be statistically significant
565 across all basins and decades. This indicates that the uncertainty from calibration conditions
566 does not merely add to the total uncertainty but also modulates the uncertainty stemming from
567 climate models, which is a critical consideration for developing robust drought management
568 strategies. In contrast, other interactions such as SSP:HC and SSP:PL were found to be not
569 significant across the basins and decades.

570

571 3.9.3 Uncertainty contribution of future hydrological drought

572 The quantification of uncertainty in future hydrological drought was conducted using ANOVA.
573 The uncertainty in future hydrological drought projections caused by SSP, GCM, and
574 hydrological modelling parameters was clearly quantified by ANOVA. Fig S.10 shows the
575 contribution of each factor to the total uncertainty. Among single-factor uncertainties, GCM
576 contributed the most, averaging over 30%. The largest contributor to the total uncertainty,
577 however, was the interaction between SSP and GCM, averaging over 50%.

578 Fig. 8 and Table 8 present the percentage contribution of hydrological modelling parameters
579 to the total uncertainty of the future 3-month SDI value. The uncertainty contribution from
580 hydrological model parameter estimation in future hydrological drought analysis averaged
581 2.7%, which is lower than that observed for future runoff projections. The uncertainty
582 contribution from hydrological model calibration for future drought conditions was highest in
583 HCH, followed by CJ, AD, and SJ, respectively. These results differ from those obtained in the
584 runoff projections. The contribution of uncertainty in hydrological drought analysis decreased

585 for AD and SJ, where uncertainty in future runoff projection due to hydrological model
586 calibration was relatively high. In contrast, HCH showed high uncertainty contributions from
587 hydrological model calibration in both runoff and drought analyses. Monthly runoff is a direct
588 physical variable with high temporal volatility. In contrast, the SDI, used here to quantify
589 hydrological drought, is a processed statistical indicator. It is calculated by accumulating and
590 standardizing runoff over multi-month timescales. This integration process acts as a filter,
591 effectively smoothing the high-frequency variability of the raw runoff series. Consequently,
592 the absolute numerical fluctuation of the SDI is significantly smaller than that of the runoff
593 itself. This reduced total variance in the drought index is the primary reason why the quantified
594 uncertainty contributions appear lower and exhibit a different pattern compared to the runoff
595 analysis. This highlights that while the underlying drivers of uncertainty are the same, their
596 manifestation can differ depending on the temporal scale and the nature of the hydrological
597 variable being analyzed. These findings confirm the necessity to separately analyze and
598 consider uncertainties in future runoff projection and hydrological drought analysis.

599

600 **4. Discussion**

601 This study quantified the cascade of uncertainties caused by various factors in the process of
602 projecting future runoff and analyzing future hydrological drought. Previous studies
603 (Chegwidden et al., 2019; Wang et al., 2020) have reported that climate data from GCMs and
604 SSP scenarios are the primary sources of uncertainty in future hydrological analysis. The
605 results of this study also identified GCMs as the major contributor to uncertainty in future
606 runoff analysis. This aligns with findings such as Her et al. (2019), who demonstrated that
607 GCM uncertainty is dominant for rapid hydrological components, whereas parameter
608 uncertainty becomes more significant for slower. However, recent research has begun to
609 identify and quantify the cascade of uncertainties caused by factors beyond GCMs and SSP
610 scenarios (Chen et al., 2022; Shi et al., 2022). This study focused on the uncertainties inherent
611 in the calibration of hydrological models, which are essential for future water resource
612 management. Rather than seeking a single optimal parameter set, the central aim of this study
613 was to quantify the uncertainty that arises from this very choice.

614 There have been limited studies that consider the uncertainties in runoff projection due to
615 various calibrated parameter cases (Lee et al., 2021a). However, this study further subdivided
616 the observation data used in the calibration period of hydrological model parameters by the

617 amount of data and hydrological conditions to quantify the uncertainties more precisely. The
618 results showed that hydrological conditions had a greater impact than the amount of calibration
619 data period on the uncertainties in the calibration of hydrological model parameters.

620 This study went beyond merely projecting future runoff by also quantifying the cascade of
621 uncertainties in the analysis of future hydrological drought using this runoff projection. Many
622 studies on future drought prediction reported that hydrological drought becomes more complex
623 and uncertain due to its association with human activities and the use of future climate data and
624 hydrological models (Ashrafi et al., 2020; Satoh et al., 2022). For example, Gao et al. (2020),
625 also using an ANOVA approach, found that for low flows, GCM and RCP uncertainty became
626 increasingly pronounced. Most existing studies on future hydrological drought analysis
627 focused on the severity and frequency of droughts. However, this study quantified the cascade
628 of uncertainties that arise in the process of future drought analysis. Although the contribution
629 of hydrological model uncertainty to future hydrological drought may be lower compared to
630 future runoff projections, the characteristics of uncertainty differ between drought and runoff
631 projections, clearly indicating the necessity to separately analyze and consider these
632 uncertainties in future hydrological analyses.

633 Furthermore, the basin-specific characteristics presented in Table S1 help interpret the differing
634 uncertainty contributions seen in the results. For example, in the hydrological drought analysis
635 (Fig. 8), the uncertainty from model calibration was highest in HCH (5.56%) but lowest in SJ
636 (0.26%), despite their similar areas (925 km² vs 763 km²). A key difference is that the SJ basin
637 receives significantly higher mean annual precipitation (1,329.8 mm) compared to HCH
638 (1,289.9 mm) and especially AD (1,045.7 mm). This suggests that basins with lower
639 precipitation (like HCH and AD) may be more hydrologically sensitive to calibration data
640 selection, leading to higher model-driven uncertainty, whereas the wetter conditions in SJ
641 create a more robust (less sensitive) hydrological response regardless of calibration choice.

642

643 **5. Conclusion**

644 This study aimed to quantify the uncertainties in future runoff projections and hydrological
645 drought analysis, considering various climate change scenarios and hydrological model
646 calibrations. SWAT was used, and hydrological conditions were classified using the SDI.
647 Additionally, 20 GCMs and three SSP scenarios were applied. The calibration data length
648 ranged from 1 to 20 years, considering different hydrological conditions (Dry, Normal, Wet).

649 The main findings are as follows:

650 First, the validation performance of the calibrated hydrological model parameters depended
651 significantly on the hydrological conditions of the calibration data. For instance, when
652 compared against parameters calibrated using wet period data, hydrological model parameters
653 calibrated with dry period data showed an average of 11.4% higher performance when
654 validated under dry conditions and 6.1% higher performance when validated under normal
655 conditions.

656 Second, the contribution of hydrological model uncertainty to future runoff projections ranged
657 from 3.9% to 9.8%, with this uncertainty being more pronounced during low runoff periods.
658 ANOVA results clearly indicated that GCMs contributed the most uncertainty, consistently
659 accounting for over 60% on average, highlighting GCMs as the dominant source. In contrast,
660 the contributions of SSP scenarios and hydrological model parameters were relatively smaller.

661 Third, the contribution of hydrological model uncertainty in future hydrological drought
662 analysis was on average 2.7%, lower than that observed for future runoff projections. The
663 uncertainty contributions varied by basin, showing different patterns from runoff projections,
664 thus confirming the necessity for separate analyses of future runoff and hydrological drought
665 uncertainties.

666 The significance of this study lies in emphasizing the quantification of uncertainty from various
667 sources, including hydrological conditions and calibration data length, in addition to climate
668 model scenarios. The systematic approach using ANOVA provided insights into the dominant
669 sources and interactions of uncertainties, offering important guidance for improving
670 hydrological modeling practices and water resources planning under future climate scenarios.
671 However, there remains a need to apply this methodology to other regions to generalize these
672 findings further.

673

674 **Code and data availability**

675 The code and data supporting the findings of this study are available upon reasonable request
676 from the corresponding author. Please contact Eun-Sung Chung (eschung@seoultech.ac.kr)
677 for further details.

678 **Author contributions**

679 E.S, Chung and J.H, Kim planned the research, J.H, Kim ran the hydrological model, E.S,
680 Chung and J.H, Kim analyzed the data, J.H, Kim wrote the manuscript draft, and E.S, Chung
681 and J.H, Kim reviewed and edited the manuscript.

682 **Competing interests**

683 The contact author has declared that none of the authors has any competing interests.

684 **Disclaimer**

685 Publisher's note: Copernicus Publications remains neutral with regard to jurisdictional claims
686 made in the text, published maps, institutional affiliations, or any other geographical
687 representation in this paper. While Copernicus Publications makes every effort to include
688 appropriate place names, the final responsibility lies with the authors. Views expressed in the
689 text are those of the authors and do not necessarily reflect the views of the publisher.

690 **Acknowledgement**

691 We would like to thank the Editor, Dr. Lelys Bravo de Guenni, and the reviewers, Dr. Francis
692 Chiew and the anonymous referee, for their comments and constructive observations, which
693 meaningfully improved the quality of this paper.

694 **Financial support**

695 This study was supported by of National Research Foundation of Korea
696 (2021R1A2C200569915).

697

698 **References**

699 Abdulai, P. J., Chung, E.S.: Uncertainty assessment in drought severities for the
700 Cheongmicheon watershed using multiple GCMs and the reliability ensemble averaging
701 method, Sustainability, 11(16), 4283, <https://doi.org/10.3390/su11164283>, 2019

702 Arsenault, R., Brissette, F., & Martel, J. L.: The hazards of split-sample validation in
703 hydrological model calibration, J Hydrol, 566, 346-362,
704 <https://doi.org/10.1016/j.jhydrol.2018.09.027>, 2018

705 Ashrafi, S. M., Gholami, H., & Najafi, M. R.: Uncertainties in runoff projection and
706 hydrological drought assessment over Gharesu basin under CMIP5 RCP
707 scenarios, *J Water Clim Chang*, 11(S1), 145-163, <https://doi.org/10.2166/wcc.2020.088>, 2020

708 Bai, P., Liu, X., & Xie, J.: Simulating runoff under changing climatic conditions: a
709 comparison of the long short-term memory network with two conceptual hydrologic
710 models, *J Hydrol*, 592, 125779, <https://doi.org/10.1016/j.jhydrol.2020.125779>, 2021

711 Bosshard, T., Carambia, M., Goergen, K., Kotlarski, S., Krahe, P., Zappa, M., & Schär, C.:
712 Quantifying uncertainty sources in an ensemble of hydrological climate-impact
713 projections, *Water Resour Res*, 49(3), 1523-1536, <https://doi.org/10.1029/2011WR011533>,
714 2013

715 Broderick, C., Matthews, T., Wilby, R. L., Bastola, S., & Murphy, C.: Transferability of
716 hydrological models and ensemble averaging methods between contrasting climatic
717 periods, *Water Resour Res*, 52(10), 8343-8373, <https://doi.org/10.1002/2016WR018850>,
718 2016

719 Chae, S. T., Chung, E. S., & Jiang, J.: Enhancing Water Cycle Restoration through LID
720 Practices Considering Climate Change: A Study on Permeable Pavement Planning by an
721 Iterative MCDM Model, *Water Resour Manag*, 38(9), 3413-3428,
722 <https://doi.org/10.1007/s11269-024-03821-z>, 2024

723 Chae, S.T. Chung, E.S., Kim, D.: Evaluation of optimized multi-model ensembles for
724 extreme precipitation projection considering various objective functions, *Water Resour*, 1-19,
725 <https://doi.org/10.1007/s11269-024-03948-z>, 2024

726 Chegwidden, O. S., Nijssen, B., Rupp, D. E., Arnold, J. R., Clark, M. P., Hamman, J. J., Kao,
727 S.-C., Mao, Y., Mizukami, N., Mote, P.W., Pan, M., Pytlak, E., & Xiao, M.: How do
728 modeling decisions affect the spread among hydrologic climate change projections?
729 Exploring a large ensemble of simulations across a diversity of hydroclimates, *Earths
730 Future*, 7(6), 623-637, <https://doi.org/10.1029/2018EF001047>, 2019

731 Chen, C., Gan, R., Feng, D., Yang, F., & Zuo, Q.: Quantifying the contribution of SWAT
732 modeling and CMIP6 inputting to streamflow prediction uncertainty under climate change, *J
733 Clean Prod*, 364, 132675, <https://doi.org/10.1016/j.jclepro.2022.132675>, 2022

734 Coron, L., Andréassian, V., Perrin, C., Lerat, J., Vaze, J., Bourqui, M., & Hendrickx, F.:
735 Crash testing hydrological models in contrasted climate conditions: An experiment on 216
736 Australian catchments, *Water Resour Res*, 48(5), <https://doi.org/10.1029/2011WR011721>,
737 2012

738 Dakhlaoui, H., Ruelland, D., Tramblay, Y., & Bargaoui, Z.: Evaluating the robustness of
739 conceptual rainfall-runoff models under climate variability in northern Tunisia, *J
740 Hydrol*, 550, 201-217, <https://doi.org/10.1016/j.jhydrol.2017.04.032>, 2017

741 Devia, G. K., Ganasri, B. P., & Dwarakish, G. S.: A review on hydrological
742 models, *Aquat Procedia*. 4, 1001-1007, <https://doi.org/10.1016/j.aqpro.2015.02.126>, 2015

743 Feng, K., Zhou, J., Liu, Y., Lu, C., & He, Z.: Hydrological uncertainty processor (HUP) with
744 estimation of the marginal distribution by a Gaussian mixture model, *Water Resour
745 Manag*, 33, 2975-2990, <https://doi.org/10.1007/s11269-019-02260-5>, 2019

746 Fowler, K. J., Peel, M. C., Western, A. W., Zhang, L., & Peterson, T. J.: Simulating runoff
747 under changing climatic conditions: Revisiting an apparent deficiency of conceptual rainfall-
748 runoff models, *Water Resour Res*. 52(3), 1820-1846,
749 <https://doi.org/10.1002/2015WR018068>, 2016

750 Gao, C., Booij, M. J., & Xu, Y. P.: Assessment of extreme flows and uncertainty under
751 climate change: disentangling the uncertainty contribution of representative concentration
752 pathways, global climate models and internal climate variability, *Hydrol Earth Syst
753 Sci*, 24(6), 3251-3269, <https://doi.org/10.5194/hess-24-3251-2020>, 2020

754 Ghasemizade, M., & Schirmer, M.: Subsurface flow contribution in the hydrological cycle:
755 lessons learned and challenges ahead—a review, *Environ Earth Sci*. 69, 707-718,
756 <https://doi.org/10.1007/s12665-013-2329-8>, 2013

757 Gudmundsson, L., Bremnes, J. B., Haugen, J. E., & Engen-Skaugen, T.: Downscaling RCM
758 precipitation to the station scale using statistical transformations—a comparison of
759 methods, *Hydrol Earth Syst Sci*, 16(9), 3383-3390, <https://doi.org/10.5194/hess-16-3383-2012>, 2012

761 Gupta, H. V., Kling, H., Yilmaz, K. K., & Martinez, G. F.: Decomposition of the mean
762 squared error and NSE performance criteria: Implications for improving hydrological
763 modelling, *J Hydrol*, 377(1-2), 80-91, <https://doi.org/10.1016/j.jhydrol.2009.08.003>, 2009

764 Hanel, M., & Buishand, T. A.: Assessment of the sources of variation in changes of
765 precipitation characteristics over the Rhine basin using a linear mixed-effects model. *J*
766 *Clim.*, 28(17), 6903-6919, <https://doi.org/10.1175/JCLI-D-14-00775.1>, 2015

767 Her, Y., Yoo, S. H., Cho, J., Hwang, S., Jeong, J., & Seong, C.: Uncertainty in hydrological
768 analysis of climate change: multi-parameter vs. multi-GCM ensemble predictions, *Sci.*
769 *Rep.*, 9(1), 4974, <https://doi.org/10.1038/s41598-019-41334-7>, 2019

770 Hong, X., Guo, S., Zhou, Y., & Xiong, L.: Uncertainties in assessing hydrological drought
771 using streamflow drought index for the upper Yangtze River basin, *Stoch Environ*
772 *Res Risk Assess*, 29, 1235-1247, <https://doi.org/10.1007/s00477-014-0949-5>, 2015

773 IPCC: *IPCC Climate Change 2014: Synthesis Report. Contribution of Working Groups I, II*
774 and III to the Fifth Assessment Report of the Intergovernmental Panel on Climate Change,
775 *IPCC*, Geneva, Switzerland, 2014

776 IPCC.: Summary for Policymakers. In: *Climate Change 2021: The Physical Science Basis.*
777 Contribution of Working Group I to the Sixth Assessment Report of the Intergovernmental
778 Panel on Climate Change [Masson-Delmotte, V., P. Zhai, A. Pirani, S. L. Connors, C. Péan,
779 S. Berger, N. Caud, Y. Chen, L. Goldfarb, M. I. Gomis, M. Huang, K. Leitzell, E. Lonnoy,
780 J.B.R. Matthews, T. K. Maycock, T. Waterfield, O. Yelekçi, R. Yu and B. Zhou (eds.)].
781 Cambridge University Press. In Press, 2021

782 Karunakalage, A., Lee, J. Y., Daqiq, M. T., Cha, J., Jang, J., & Kannaujiya, S.:
783 Characterization of groundwater drought and understanding of climatic impact on
784 groundwater resources in Korea, *J Hydrol.*, 634, 131014,
785 <https://doi.org/10.1016/j.jhydrol.2024.131014>, 2024

786 Kim, H. S., Croke, B. F., Jakeman, A. J., & Chiew, F. H.: An assessment of modelling
787 capacity to identify the impacts of climate variability on catchment hydrology, *Math Comput*
788 *Simul.* 81(7), 1419-1429, <https://doi.org/10.1016/j.matcom.2010.05.007>, 2011

789 Kim, J. H., Sung, J. H., Chung, E. S., Kim, S. U., Son, M., & Shiru, M. S.: Comparison of
790 Projection in Meteorological and Hydrological Droughts in the Cheongmicheon Watershed
791 for RCP4. 5 and SSP2-4.5, *Sustainability*, 13(4), 2066, <https://doi.org/10.3390/su13042066>,
792 2021

793 Kim, J. H., Sung, J. H., Shahid, S., & Chung, E. S.: Future hydrological drought analysis
794 considering agricultural water withdrawal under SSP scenarios, *Water Resour Manag*, 36(9),
795 2913-2930, <https://doi.org/10.1007/s11269-022-03116-1>, 2022

796 Lee, S., Qi, J., McCarty, G. W., Yeo, I. Y., Zhang, X., Moglen, G. E., & Du, L.: Uncertainty
797 assessment of multi-parameter, multi-GCM, and multi-RCP simulations for streamflow and
798 non-floodplain wetland (NFW) water storage, *J Hydrol*, 600, 126564,
799 <https://doi.org/10.1016/j.jhydrol.2021.126564>, 2021

800 Lee, S., Lee, S. J., Jang, K., & Chun, J. H.: Drought monitoring based on vegetation type and
801 reanalysis data in Korea, *Atmosphere*, 12(2), 170,
802 <https://doi.org/10.1016/j.jhydrol.2021.126564>, 2021

803 Mahabadi, S. A., & Delavar, M.: Evaluation and comparison of different methods for
804 determining the contribution of climatic factors and direct human interventions in reducing
805 basin discharge, *Ecol Indic*, 158, 111480, <https://doi.org/10.1016/j.ecolind.2023.111480>,
806 2024

807 Merz, R., Parajka, J., & Blöschl, G.: Time stability of catchment model parameters:
808 Implications for climate impact analyses, *Water Resour Res*, 47(2),
809 <https://doi.org/10.1029/2010WR009505>, 2011

810 Milly, P. C., Betancourt, J., Falkenmark, M., Hirsch, R. M., Kundzewicz, Z. W., Lettenmaier,
811 D. P., & Stouffer, R. J., 2008. Stationarity is dead: Whither water
812 management?. *Science*. 319(5863), 573-574.

813 Mo, C., Huang, K., Ruan, Y., Lai, S., & Lei, X.: Quantifying uncertainty sources in runoff
814 change attribution based on the Budyko framework, *J Hydrol*, 630, 130790,
815 <https://doi.org/10.1016/j.jhydrol.2024.130790>, 2024

816 Morim, J., M. Hemer, X.L. Wang, N. Cartwright, C. Trenham, A. Semedo, I. Young, L.
817 Bricheno, P. Camus, M. Casas-Prat, L.i. Erikson, L. Mentaschi, N. Mori, T. Shimura, B.
818 Timmermans, O. Aarnes, Ø. Breivik, A. Behrens, M. Dobrynin, M. Menendez, J. Staneva, M.
819 Wehner, J. Wolf, B. Kamranzad, A. Webb, J. Stopa, F. Andutta.: Robustness and
820 uncertainties in global multivariate wind-wave climate projections, *Nat Clim Chang*, 9(9),
821 711-718, <https://doi.org/10.1038/s41558-019-0542-5>, 2019

822 Nalbantis, I., & Tsakiris, G.: Assessment of hydrological drought revisited, *Water Resour*
823 *Manag*, 23, 881-897, <https://doi.org/10.1007/s11269-008-9305-1>, 2009

824 Nguyen, T. V., Dietrich, J., Dang, T. D., Tran, D. A., Van Doan, B., Sarrazin, F. J.,
825 Abbaspour, K., & Srinivasan, R.: An interactive graphical interface tool for parameter
826 calibration, sensitivity analysis, uncertainty analysis, and visualization for the Soil and Water
827 Assessment Tool, *Environ Model Softw*, 156, 105497,
828 <https://doi.org/10.1016/j.envsoft.2022.105497>, 2022

829 O'Neill, B. C., Tebaldi, C., Van Vuuren, D. P., Eyring, V., Friedlingstein, P., Hurtt, G.,
830 Knutti, R., Kriegler, E., Lamarque, J.F., Lowe, J., Meehl, J., Moss, R., Riahi, K., Sanderson,
831 B. M.: The scenario model intercomparison project (ScenarioMIP) for
832 CMIP6, *Geosci Model Dev*, 9(9), 3461-3482, <https://doi.org/10.5194/gmd-9-3461-2016>,
833 2016

834 Peng, A., Zhang, X., Xu, W., & Tian, Y.: Effects of training data on the learning performance
835 of LSTM network for runoff simulation, *Water Resour Manag*, 36(7), 2381-2394,
836 <https://doi.org/10.1007/s11269-022-03148-7>, 2022

837 Perrin, C., Oudin, L., Andreassian, V., Rojas-Serna, C., Michel, C., & Mathevet, T.: Impact
838 of limited streamflow data on the efficiency and the parameters of rainfall—runoff
839 models, *Hydrol Sci J*, 52(1), 131-151, <https://doi.org/10.1623/hysj.52.1.131>, 2007

840 Qi, W., Zhang, C., Fu, G., Sweetapple, C., & Zhou, H.: Evaluation of global fine-resolution
841 precipitation products and their uncertainty quantification in ensemble discharge
842 simulations, *Hydrol Earth Syst Sci*, 20(2), 903-920, <https://doi.org/10.5194/hess-20-903>,
843 2016, 2016

844 Razavi, S., & Tolson, B. A.: An efficient framework for hydrologic model calibration on long
845 data periods, *Water Resour Res*, 49(12), 8418-8431, <https://doi.org/10.1002/2012WR013442>,
846 2013

847 Renard, B., Kavetski, D., Kuczera, G., Thyer, M., & Franks, S. W.: Understanding predictive
848 uncertainty in hydrologic modeling: The challenge of identifying input and structural
849 errors, *Water Resour Res*, 46(5), <https://doi.org/10.1029/2009WR008328>, 2010

850 Saft, M., Peel, M. C., Western, A. W., Perraud, J. M., & Zhang, L.: Bias in streamflow
851 projections due to climate-induced shifts in catchment response, *Geophys Res Lett*, 43(4),
852 1574-1581, <https://doi.org/10.1002/2015GL067326>, 2016

853 Santos, C. A. G., Neto, R. M. B., do Nascimento, T. V. M., da Silva, R. M., Mishra, M., &
854 Frade, T. G.: Geospatial drought severity analysis based on PERSIANN-CDR-estimated
855 rainfall data for Odisha state in India (1983–2018), *Sci Total Environ*, 750, 141258,
856 <https://doi.org/10.1016/j.scitotenv.2020.141258>, 2021

857 Satoh, Y., Yoshimura, K., Pokhrel, Y., Kim, H., Shiogama, H., Yokohata, T., Hanasaki, N.,
858 Wada, Y., Burek, P., Byers, E., Schmied, H. M., Gerten, D., Ostberg, S., Gosling, S. N.,
859 Boulange, J. E. S., & Oki, T.: The timing of unprecedented hydrological drought under
860 climate change, *Nat Commun*, 13(1), 3287, <https://doi.org/10.1038/s41467-022-30729-2>,
861 2022

862 Sheffield, J., & Wood, E. F.: Drought: past problems and future scenarios. Routledge,
863 <https://doi.org/10.4324/9781849775250>, 2012

864 Shi, L., Feng, P., Wang, B., Li Liu, D., Zhang, H., Liu, J., & Yu, Q.: Assessing future runoff
865 changes with different potential evapotranspiration inputs based on multi-model ensemble of
866 CMIP5 projections, *J Hydrol*, 612, 128042, <https://doi.org/10.1016/j.jhydrol.2022.128042>,
867 2022

868 Song, Y. H., Chung, E. S., & Shahid, S.: Differences in extremes and uncertainties in future
869 runoff simulations using SWAT and LSTM for SSP scenarios, *Sci Total Environ*, 838,
870 156162, <https://doi.org/10.1016/j.scitotenv.2022.156162>, 2022

871 Sun, W., Wang, Y., Wang, G., Cui, X., Yu, J., Zuo, D., & Xu, Z.: Physically based
872 distributed hydrological model calibration based on a short period of streamflow data: case
873 studies in four Chinese basins, *Hydrol Earth Syst Sci*, 21(1), 251-265,
874 <https://doi.org/10.5194/hess-21-251-2017>, 2017

875 Sung, J. H., Chung, E. S., & Shahid, S.: Reliability–Resiliency–Vulnerability approach for
876 drought analysis in South Korea using 28 GCMs, *Sustainability*, 10(9), 3043,
877 <https://doi.org/10.3390/su10093043>, 2018

878 Thirel, G., Andréassian, V., & Perrin, C.: On the need to test hydrological models under
879 changing conditions, *Hydrol Sci J*, 60(7-8), 1165-1173,
880 <https://doi.org/10.1080/02626667.2015.1050027>, 2015

881 Vetter, T., Huang, S., Aich, V., Yang, T., Wang, X., Krysanova, V., & Hattermann, F.: Multi-
882 model climate impact assessment and intercomparison for three large-scale river basins on
883 three continents, *Earth Syst Dyn*, 6(1), 17-43, <https://doi.org/10.5194/esd-6-17-2015>, 2015

884 Wang, H. M., Chen, J., Xu, C. Y., Zhang, J., & Chen, H.: A framework to quantify the
885 uncertainty contribution of GCMs over multiple sources in hydrological impacts of climate
886 change, *Earth's Future*, 8(8), e2020EF001602, <https://doi.org/10.1029/2020EF001602>, 2020

887 Xu, Z., Godrej, A. N., & Grizzard, T. J.: The hydrological calibration and validation of a
888 complexly-linked watershed-reservoir model for the Occoquan watershed, Virginia, *J
889 Hydrol*, 345(3-4), 167-183, <https://doi.org/10.1016/j.jhydrol.2007.07.015>, 2007

890 Yang, G., Giuliani, M., & Galelli, S.: Valuing the codesign of streamflow forecast and
891 reservoir operation models, *J Water Resour Plan Manag*, 149(8), 04023037,
892 <https://doi.org/10.1061/JWRMD5.WRENG-6023>, 2023

893 Yang, X., Chen, Z., & Qin, M.: Monthly Runoff Prediction Via Mode Decomposition-
894 Recombination Technique, *Water Resour Manag*, 38(1), 269-286,
895 <https://doi.org/10.1007/s11269-023-03668-w>, 2023

896 Yip, S., Ferro, C. A., Stephenson, D. B., & Hawkins, E.: A simple, coherent framework for
897 partitioning uncertainty in climate predictions, *J Clim Change*, 24(17), 4634-4643,
898 <https://doi.org/10.1175/2011JCLI4085.1>, 2011

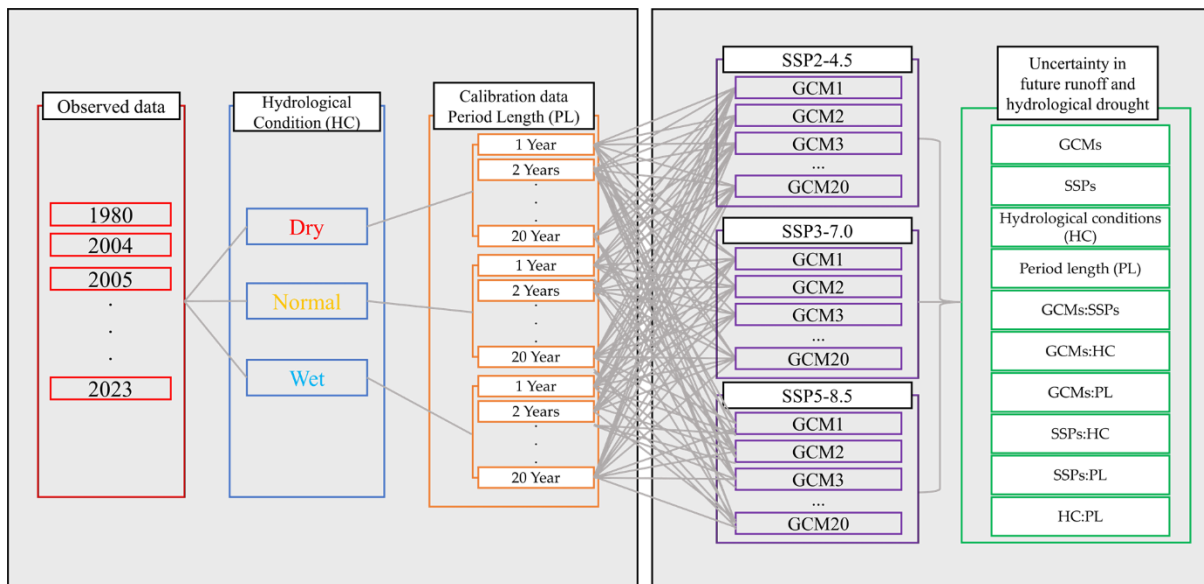
899 Yu, Q., Jiang, L., Wang, Y., & Liu, J., 2023. Enhancing streamflow simulation using
900 hybridized machine learning models in a semi-arid basin of the Chinese loess Plateau. *J
901 Hydrol*. 617, 129115.

902 Yuan, Q., Thorarinsdottir, T. L., Beldring, S., Wong, W. K., & Xu, C. Y.: Assessing
903 uncertainty in hydrological projections arising from local-scale internal variability of
904 climate, *J Hydrol*, 620, 129415, <https://doi.org/10.1016/j.jhydrol.2023.129415>, 2023

905 Zhang, X., Song, S., & Guo, T.: Nonlinear Segmental Runoff Ensemble Prediction Model
906 Using BMA, *Water Resour Manag*, 1-18, <https://doi.org/10.1007/s11269-024-03824-w>, 2024

907 Ziarh, G. F., Kim, J. H., Song, J. Y., & Chung, E. S.: Quantifying Uncertainty in Runoff
908 Simulation According to Multiple Evaluation Metrics and Varying Calibration Data
909 Length, Water, 16(4), 517, <https://doi.org/10.3390/w16040517>, 2024

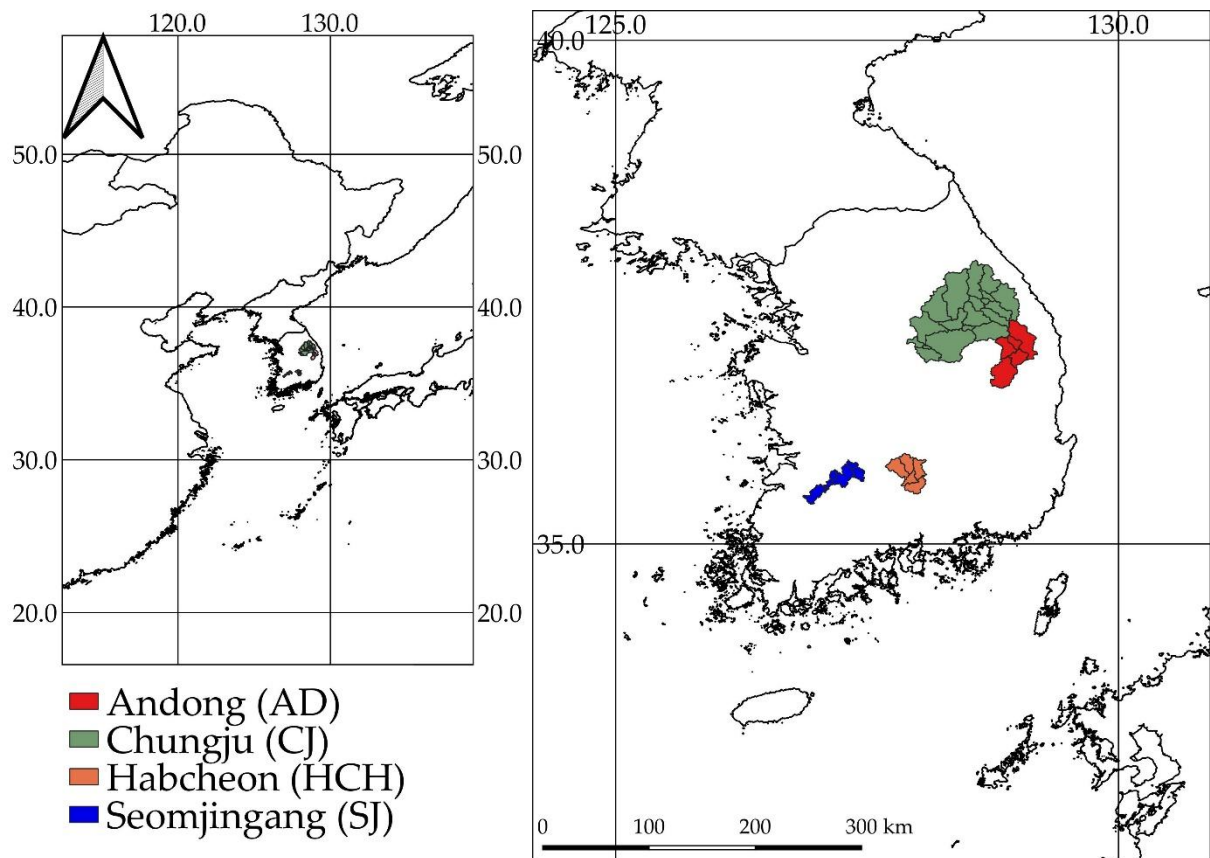
910

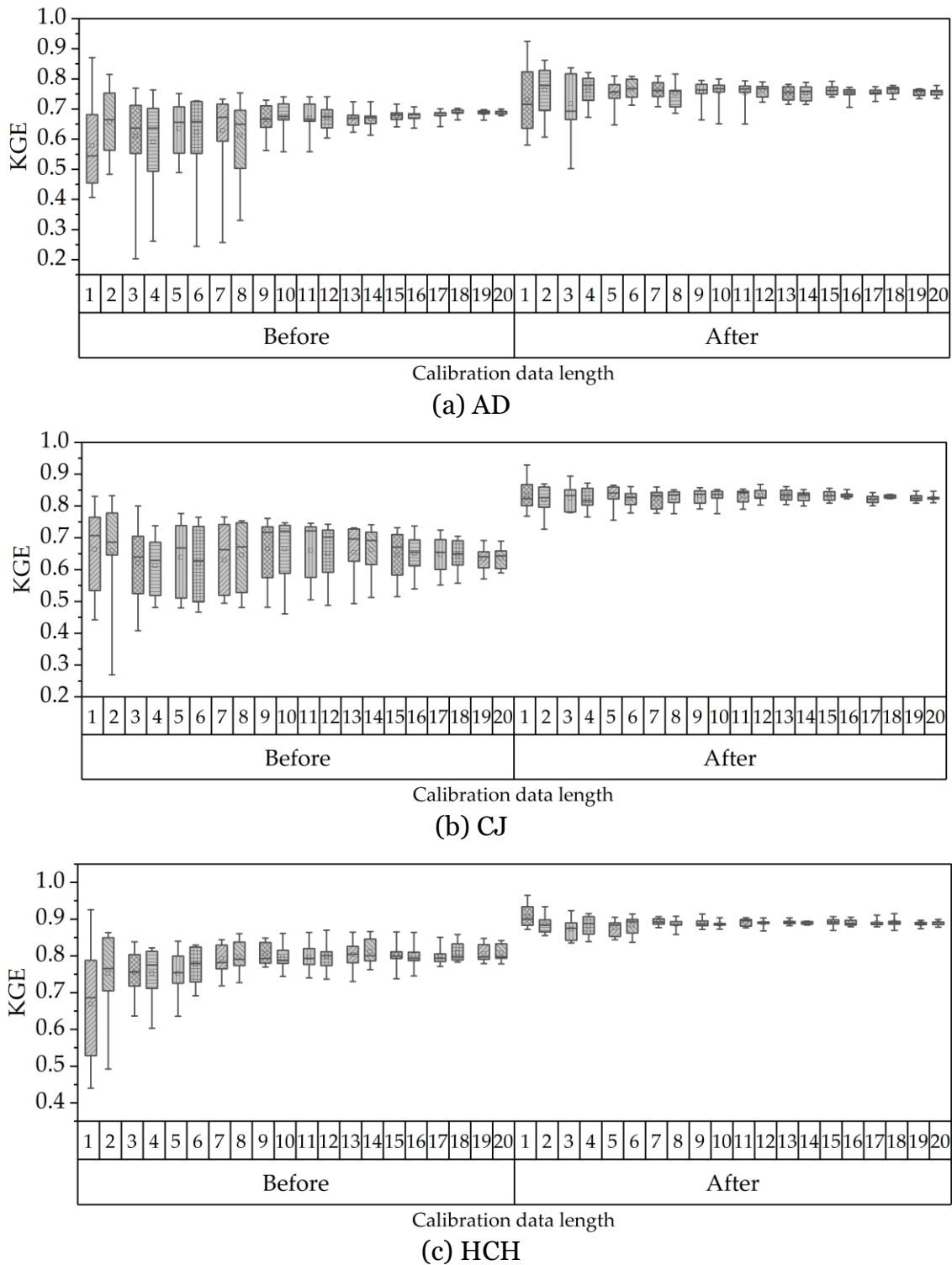


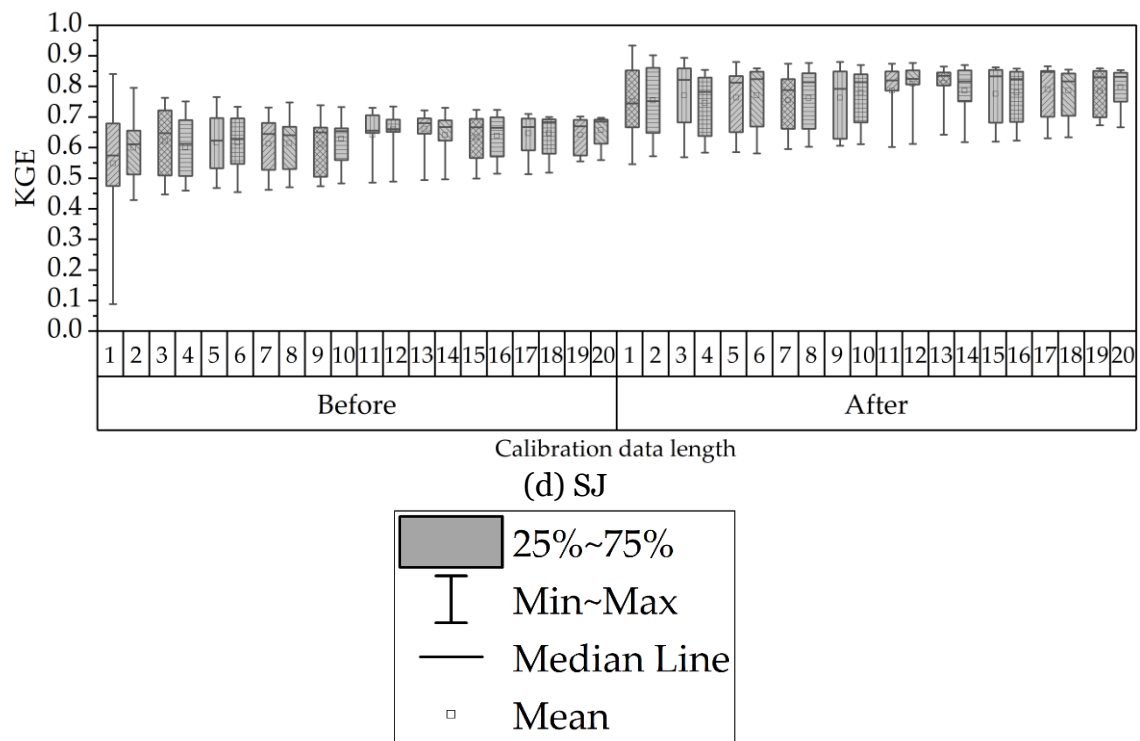
911

912 *Figure. 1. Uncertainty concept in this study*

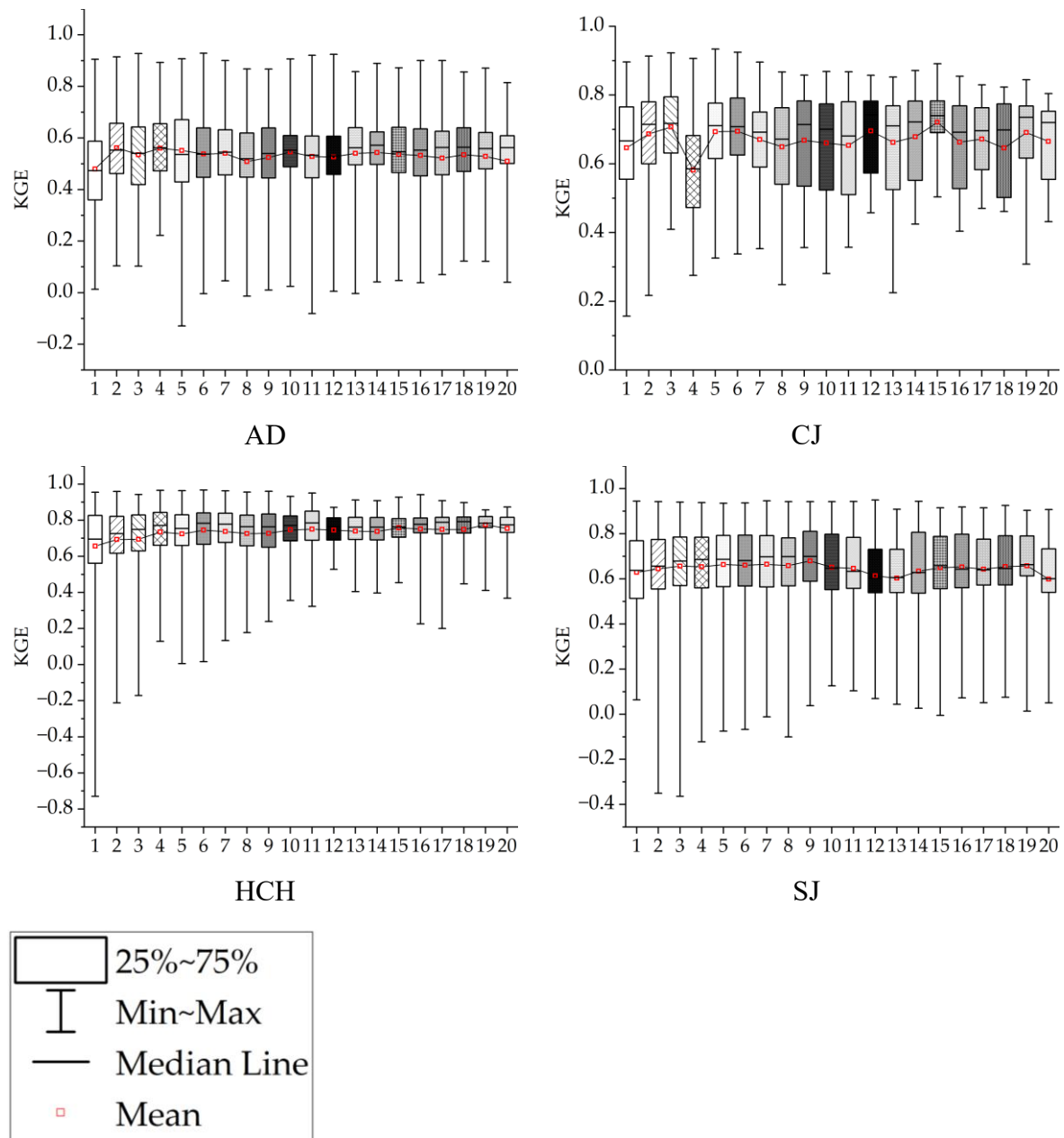
913

916 *Figure. 2. Description of study area.*



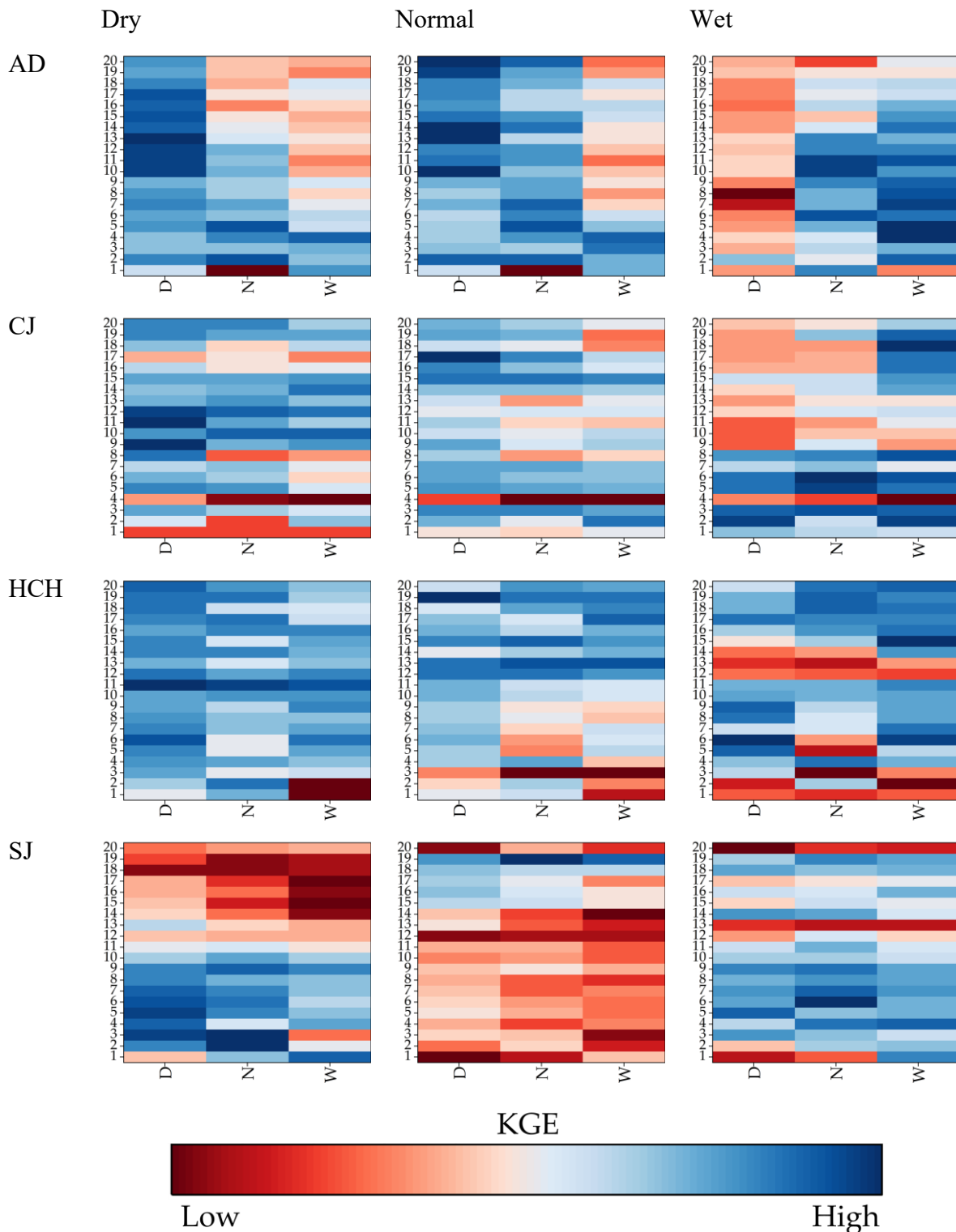


919 *Figure. 3. Comparison of KGE values for the four basins using default parameters (Before)*
 920 *and calibrated parameters (After). The x-axis (1-20) represents the calibration data length,*
 921 *which defines the before calibration/after calibration data split.*

923 *Figure. 4. Validation performances depending on data length of the calibration period*

925

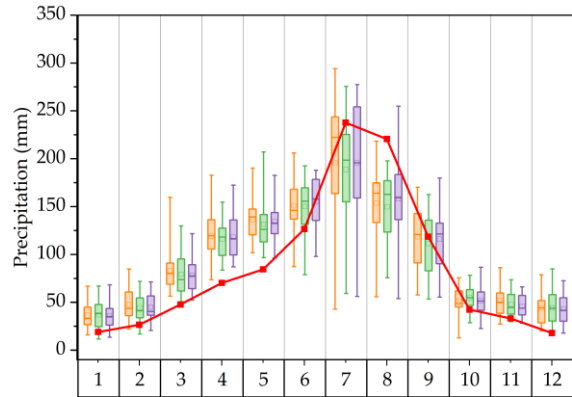
Basins Hydrological conditions for validation period



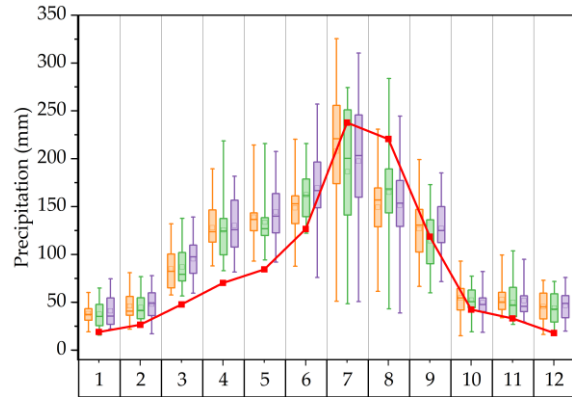
926 *Figure. 5. Heatmap matrix of KGE performance by calibration and validation conditions.*
927 *The four main rows represent the basins (AD, CJ, HC, SJ). The three main columns (labeled*
928 *'Dry', 'Normal', 'Wet') represent the hydrological conditions of the validation period. Within*

929 *each individual heatmap, the y-axis represents the calibration data length (1-20 years), and*
930 *the x-axis (labeled D, N, W) represents the hydrological conditions of the calibration period.*
931 *Blue indicates high KGE (good performance) and red indicates low KGE (poor*
932 *performance).*

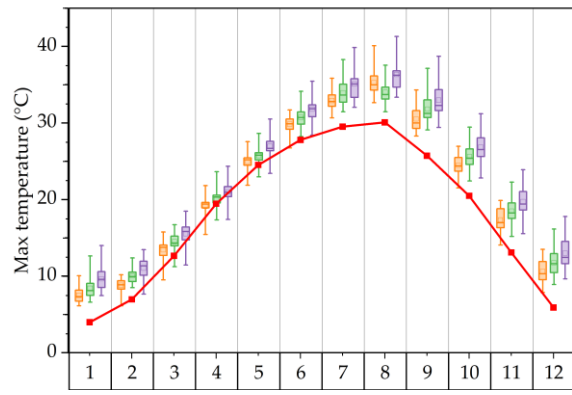
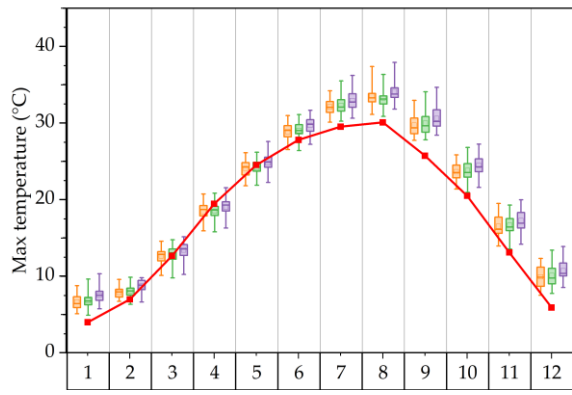
NF



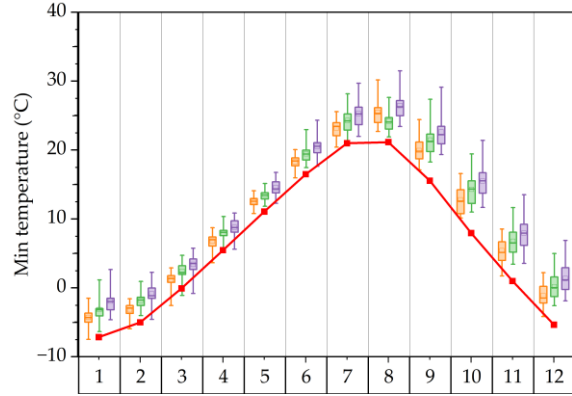
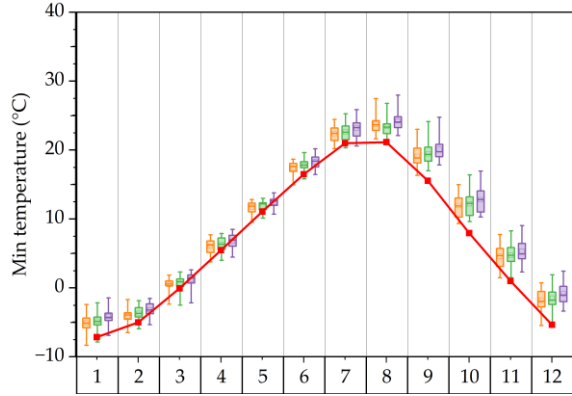
DF



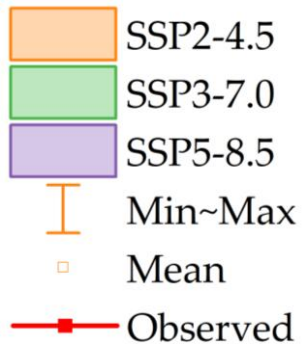
(a) Precipitation



(b) Max temperature



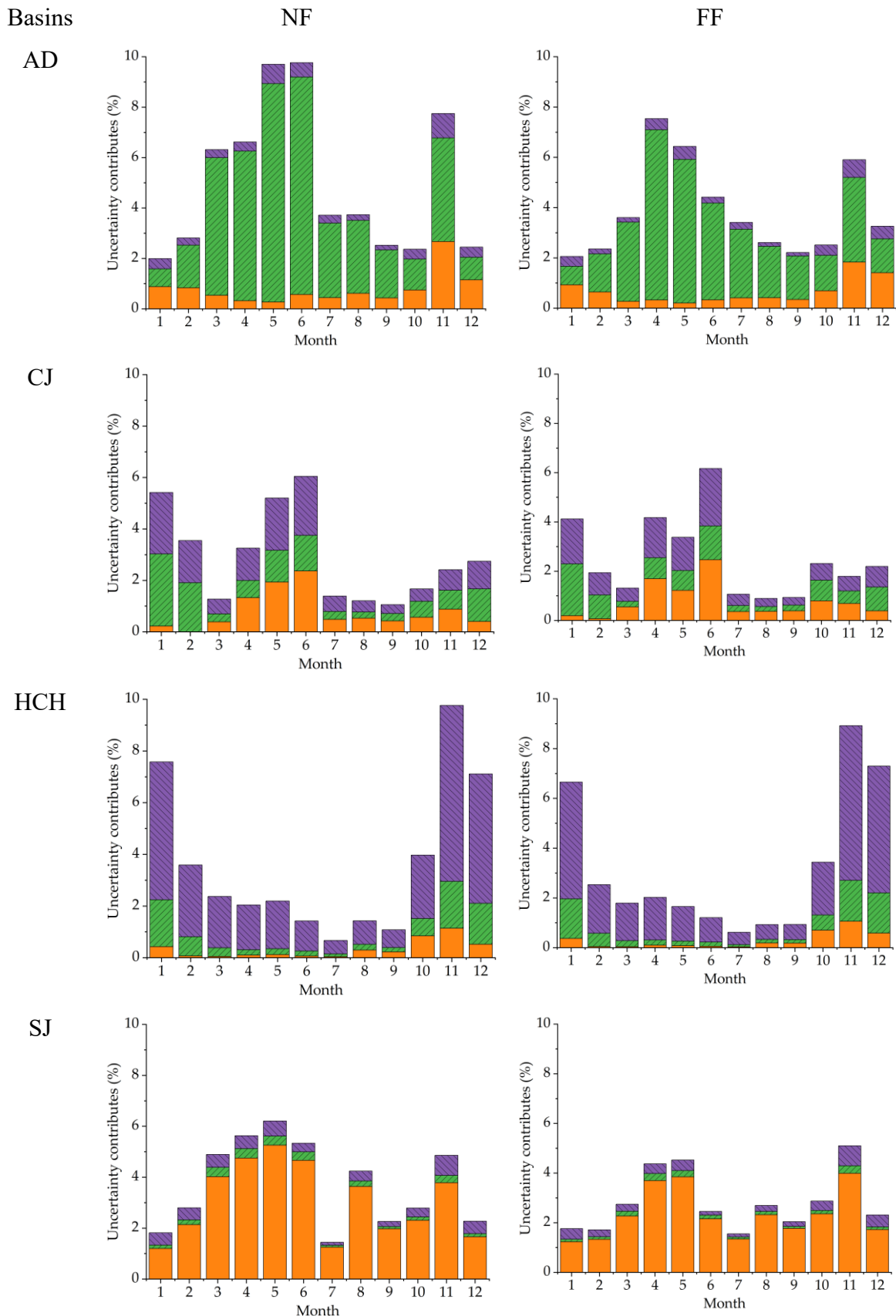
(c) Min temperature

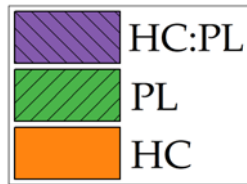


934

935 *Figure. 6. Projected annual changes in future precipitation (mm) and temperature (°C)*

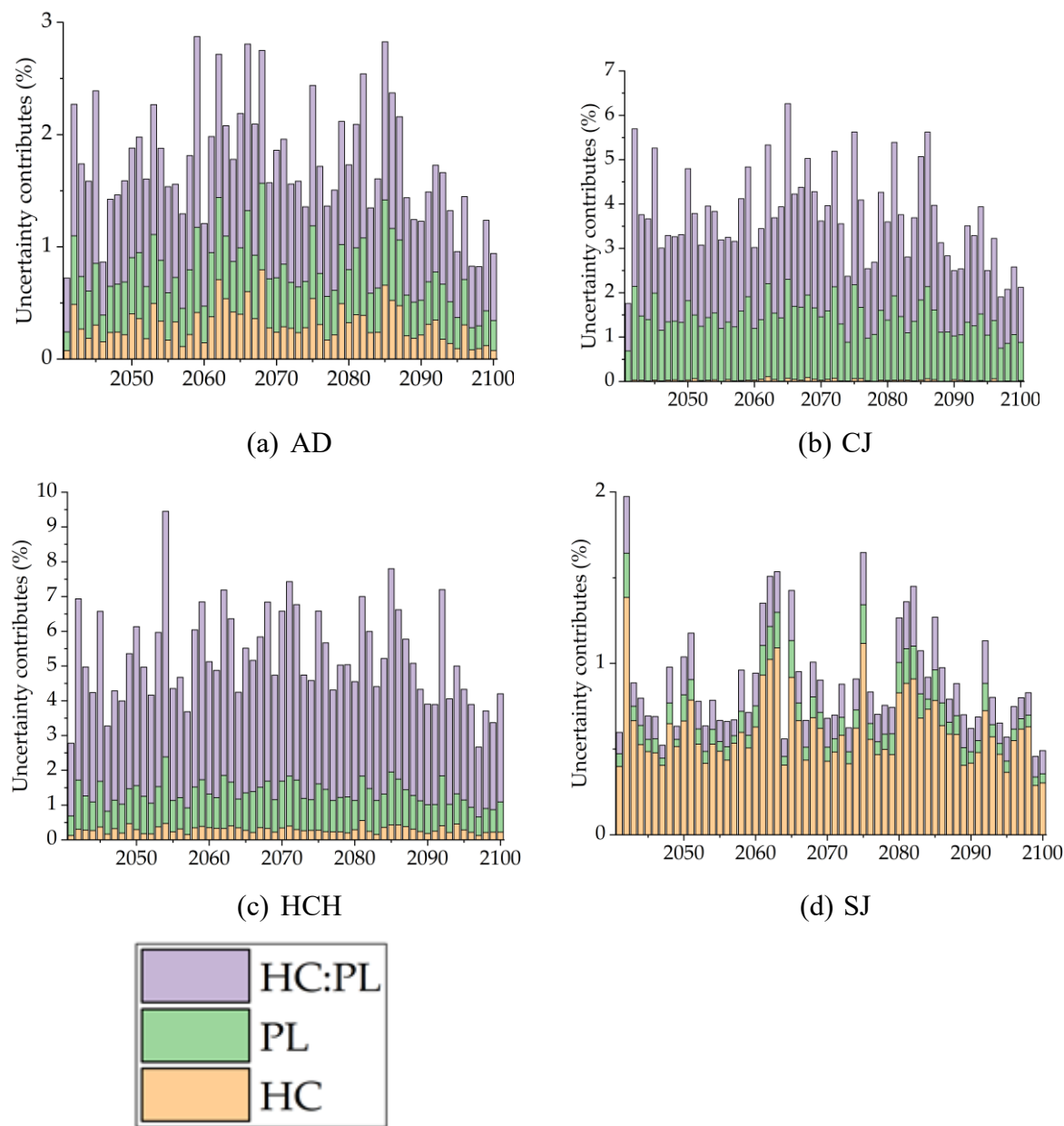
936





938 *Figure. 7. Contribution of hydrological model parameter to uncertainty in future runoff*
939 *projection using ANOVA*

940



943 *Figure. 8. Contribution of hydrological model parameters to the total uncertainty in the*
 944 *future 3-month SDI.*

945

946

Table 1. Validation performance according to hydrological conditions

Basins	Validation climatic conditions	Calibration period hydrological conditions		
		D	N	W
AD	D	0.480	0.401	0.382
	N	0.573	0.562	0.510
	W	0.571	0.621	0.642
CJ	D	0.743	0.727	0.725
	N	0.643	0.621	0.615
	W	0.674	0.686	0.706
HCH	D	0.732	0.691	0.670
	N	0.738	0.719	0.714
	W	0.763	0.757	0.769
SJ	D	0.557	0.544	0.515
	N	0.677	0.671	0.650
	W	0.674	0.681	0.684

947

948

949

Table 2. Changes from historical to future runoff for four dam basins

950

(unit: %)

Basins	SSPs	NF				DF			
		Spring	Summer	Fall	Winter	Spring	Summer	Fall	Winter
AD	SSP2-4.5	82.1	-9.9	10.8	178.3	92.6	-5.3	18.1	179.2
	SSP3-7.0	84.3	-11.1	6.7	168.3	104.3	-6.3	16.4	188.9
	SSP5-8.5	91.0	-5.7	12.9	194.2	118.9	1.2	26.7	216.1
CJ	SSP2-4.5	184.6	25.1	34.7	242.8	191.7	32.4	47.3	252.7
	SSP3-7.0	186.6	21.0	32.8	226.7	210.2	27.6	44.7	276.5
	SSP5-8.5	148.8	8.0	0.8	173.1	157.2	14.0	13.1	192.0
HCH	SSP2-4.5	207.6	2.7	-19.7	95.4	222.7	8.1	-12.3	100.8
	SSP3-7.0	213.7	-1.3	-22.5	91.2	243.4	6.8	-12.7	109.0
	SSP5-8.5	223.2	5.7	-15.2	110.0	268.8	14.8	-3.3	127.4
SJ	SSP2-4.5	170.9	1.5	7.7	60.5	181.4	5.9	18.4	63.3
	SSP3-7.0	175.1	-2.1	7.3	58.6	198.9	5.6	17.9	75.6
	SSP5-8.5	181.1	5.5	12.9	75.1	217.2	14.0	29.7	88.6

951

952

953 *Table 3. Differences in projected low-flow (Q75) based on HC. Q75 Differ (m³/s) is the*
 954 *difference (range, max-min) in the magnitude of projected Q75 (75% exceedance flow)*
 955 *values when comparing results from models calibrated under different hydrological*
 956 *conditions (Dry, Normal, and Wet).*

957 (unit: m^3/s)

Basins	SSPs	NF		DF	
		Q ₇₅ Differ	Ratio (%)	Q ₇₅ Differ	Ratio (%)
AD	SSP2-4.5	7.24	10.28	7.00	10.42
	SSP3-7.0	7.04	9.58	7.71	9.56
	SSP5-8.5	7.43	9.32	7.88	9.94
CJ	SSP2-4.5	48.93	5.60	49.00	5.35
	SSP3-7.0	48.80	4.60	52.35	5.53
	SSP5-8.5	39.02	5.70	38.09	6.11
HCH	SSP2-4.5	5.84	12.67	5.86	13.93
	SSP3-7.0	5.55	13.86	5.95	12.86
	SSP5-8.5	6.03	12.86	6.44	14.62
SJ	SSP2-4.5	4.61	9.84	4.51	9.61
	SSP3-7.0	4.23	11.24	4.64	9.76
	SSP5-8.5	4.64	9.37	4.97	9.12

958

959

960 *Table 4. Frequency of statistical significance ($p < 0.05$) of uncertainty sources for future*
 961 *monthly runoff during the NF period*

Factor	Jan	Feb	Mar	Apr	May	Jun	Jul	Aug	Sep	Oct	Nov	Dec
GCM	4/4	4/4	4/4	4/4	4/4	4/4	4/4	4/4	4/4	4/4	4/4	4/4
SSP	4/4	4/4	4/4	4/4	4/4	4/4	4/4	4/4	4/4	4/4	4/4	4/4
HC	4/4	4/4	4/4	4/4	4/4	4/4	4/4	4/4	4/4	4/4	4/4	4/4
PL	4/4	4/4	4/4	4/4	4/4	4/4	4/4	4/4	4/4	4/4	4/4	4/4
GCM:SSP	4/4	4/4	4/4	4/4	4/4	4/4	4/4	4/4	4/4	4/4	4/4	4/4
GCM:HC	3/4	2/4	2/4	2/4	2/4	4/4	4/4	4/4	4/4	4/4	4/4	4/4
GCM:PL	4/4	4/4	4/4	4/4	4/4	4/4	4/4	4/4	4/4	4/4	4/4	4/4
SSP:HC	0/4	0/4	0/4	0/4	0/4	0/4	0/4	0/4	0/4	1/4	1/4	0/4
SSP:PL	0/4	0/4	0/4	0/4	0/4	1/4	2/4	1/4	0/4	1/4	0/4	0/4
HC:PL	4/4	4/4	4/4	4/4	4/4	4/4	4/4	4/4	4/4	4/4	4/4	4/4

962

963 *Table 5. Frequency of statistical significance ($p < 0.05$) of uncertainty sources for future*
 964 *monthly runoff during the DF period*

Factor	Jan	Feb	Mar	Apr	May	Jun	Jul	Aug	Sep	Oct	Nov	Dec
GCM	4/4	4/4	4/4	4/4	4/4	4/4	4/4	4/4	4/4	4/4	4/4	4/4
SSP	4/4	4/4	4/4	4/4	4/4	4/4	4/4	4/4	4/4	4/4	4/4	4/4
HC	4/4	4/4	4/4	4/4	4/4	4/4	4/4	4/4	4/4	4/4	4/4	4/4
PL	4/4	4/4	4/4	4/4	4/4	4/4	4/4	4/4	4/4	4/4	4/4	4/4
GCM:SSP	4/4	4/4	4/4	4/4	4/4	4/4	4/4	4/4	4/4	4/4	4/4	4/4
GCM:HC	4/4	4/4	4/4	4/4	4/4	4/4	4/4	4/4	4/4	4/4	4/4	4/4
GCM:PL	4/4	4/4	4/4	4/4	4/4	4/4	4/4	4/4	4/4	4/4	4/4	4/4
SSP:HC	0/4	0/4	0/4	0/4	0/4	0/4	0/4	0/4	0/4	0/4	0/4	0/4
SSP:PL	0/4	0/4	0/4	0/4	0/4	0/4	0/4	0/4	0/4	0/4	0/4	0/4
HC:PL	4/4	4/4	4/4	4/4	4/4	4/4	4/4	4/4	4/4	4/4	4/4	4/4

965

966 *Table 6. Differences in the number of drought events according to hydrological conditions*

967 (unit: occurrences)

SSPs	Basin	AD			CJ		
		Duration	3	6	12	3	6
245	NF	5.65	1.65	0.10	1.60	0.55	0.15
	DF	4.80	0.90	0.30	1.65	0.85	0.45
370	NF	6.25	1.65	0.45	1.60	0.20	0.55
	DF	4.35	0.90	0.25	1.85	0.55	0.30
585	NF	3.95	1.65	0.25	2.35	0.50	0.40
	DF	4.55	0.90	0.20	1.75	0.65	0.60
SSPs	Basin	HCH			SJ		
		Duration	3	6	12	3	6
245	NF	0.40	0.25	0.10	1.45	0.60	0.15
	DF	0.45	1.25	0.85	2.00	0.30	0.10
370	NF	0.50	0.45	0.45	1.45	0.85	0.25
	DF	0.15	0.40	0.30	1.95	0.10	0.10
585	NF	0.55	0.20	0.15	2.50	0.30	0.35
	DF	0.45	0.30	0.50	1.65	0.35	0.30

968

969

970 *Table 7. Frequency of statistical significance ($p < 0.05$) of uncertainty sources for future*
 971 *hydrological drought*

Factor	2040s	2050s	2060s	2070s	2080s	2090s
GCM	4/4	4/4	4/4	4/4	4/4	4/4
SSP	4/4	4/4	4/4	4/4	4/4	4/4
HC	4/4	4/4	4/4	4/4	4/4	4/4
PL	4/4	4/4	4/4	4/4	4/4	4/4
GCM:SSP	4/4	4/4	4/4	4/4	4/4	4/4
GCM:HC	4/4	4/4	4/4	4/4	4/4	4/4
GCM:PL	4/4	4/4	4/4	4/4	4/4	4/4
SSP:HC	0/4	0/4	0/4	0/4	0/4	0/4
SSP:PL	0/4	0/4	0/4	0/4	0/4	0/4
HC:PL	4/4	4/4	4/4	4/4	4/4	4/4

972

Table 8. Uncertainty contribution in future hydrological drought analysis from hydrological model calibration

975 (unit: %)

Basins	NF	DF
AD	1.89	1.64
CJ	4.06	3.58
HCH	5.56	5.27
SJ	0.26	0.26

976

977